D3.15 Evaluation report aft-ship replacement: “Ernst Kramer”

Synergetics | Synergies for Green Transformation of Inland and Coastal Shipping

GRANT AGREEMENT NO.	101096809
DURATION OF THE PROJECT	42 months
DELIVERABLE NUMBER	D3.15
DISSEMINATION LEVEL	Public
DELIVERABLE LEADER	DST
STATUS	FINAL
SUBMISSION DATE	30-06-2025
AUTHORS	Friederike Dahlke-Wallat - DST Marko Josipović - DST Jan Kaufmann – DST

Funded by the Horizon Europe Programme of the European Union under grant agreement No 101096809
Funded by the Horizon Europe guarantee of the United Kingdom, under project No 10068310
Funded by the Swiss State Secretariat for Education, Research and Innovation

Table of Content

Funded by the Horizon Europe Programme of the European Union under grant agreement No 101096809
Funded by the Horizon Europe guarantee of the United Kingdom, under project No 10068310
Funded by the Swiss State Secretariat for Education, Research and Innovation

List of Figures

Funded by the Horizon Europe Programme of the European Union under grant agreement No 101096809
Funded by the Horizon Europe guarantee of the United Kingdom, under project No 10068310
Funded by the Swiss State Secretariat for Education, Research and Innovation

List of Tables

Funded by the Horizon Europe Programme of the European Union under grant agreement No 101096809
Funded by the Horizon Europe guarantee of the United Kingdom, under project No 10068310
Funded by the Swiss State Secretariat for Education, Research and Innovation

List of Abbreviations

1 | List of abbreviations.

Abbreviation	Definition
ENI	European Number of Identification
WP	Work Package
ITTC	International Towing Tank Conference
CFD	Computational Fluid Dynamics
RANS	Reynolds-Averaged Navier–Stokes
SST	Shear Stress Transport (turbulence model)
MULES	Multidimensional Universal Limiter for Explicit Solution
PISO	Pressure-Implicit Split Operator
SIMPLE	Semi-Implicit Method for Pressure-Linked Equations
PIMPLE	Combination of PISO and SIMPLE algorithms
FVM	Finite Volume Method
VoF	Volume of Fluid
CAESES	Computer-Aided Engineering for Simulation Engineering Systems
DSE	Design Space Exploration
RS	Response Surface
MOGA	Multi-Objective Genetic Algorithm
DC	Design Conditions
LC	Loading Condition
MV	Motor Vessel
CEMT	Classification of European Inland Waterways
CCNR	Central Commission for Navigation on the Rhine
PTI	Power Take-In
RBF	Radial Basis Function (morphing technique)

Funded by the Horizon Europe Programme of the European Union under grant agreement No 101096809
Funded by the Horizon Europe guarantee of the United Kingdom, under project No 10068310
Funded by the Swiss State Secretariat for Education, Research and Innovation

SLERP	Spherical Linear Interpolation
SOBOL	Quasi-random sequence used in sampling design variables
NURBS	Non-Uniform Rational B-Splines
PS	Pferdestärke (metric horsepower)
CO_2	Carbon Dioxide
PM	Particulate Matter

List of Symbols

2 | List of symbols.

Symbol	Description	Unit
$\boldsymbol{V}$	Vessel Speed	km/h
$\boldsymbol{h}$	Water Depth	m
$\boldsymbol{T}$	Mean Draft	m
$\boldsymbol{T_A}, \boldsymbol{T_F}$	Draught at Aft / Forward Perpendicular	m
$\boldsymbol{Fr_h}$	Depth Froude number	–
$\boldsymbol{h/T}$	Depth-to-draft ratio	–
$\boldsymbol{P_D}$	Delivered Power	kW

Funded by the Horizon Europe Programme of the European Union under grant agreement No 101096809
Funded by the Horizon Europe guarantee of the United Kingdom, under project No 10068310
Funded by the Swiss State Secretariat for Education, Research and Innovation

Release Approval

3 | Release approval.

Name	Role	Date
R. Graf-Potthoff (RHENUS)	Reviewer 1	27-06-2025
L. Reckers (RHENUS)	Reviewer 2	26-06-2025
B. Starke (MARIN)	Reviewer 3	27-06-2025
P. Garcia Barrena (MARIN)	WP-Leader	30-06-2025
B. Friedhoff (DST)	Coordinator	30-06-2025

Funded by the Horizon Europe Programme of the European Union under grant agreement No 101096809
Funded by the Horizon Europe guarantee of the United Kingdom, under project No 10068310
Funded by the Swiss State Secretariat for Education, Research and Innovation

Executive Summary

This case study demonstrates that achieving the CCNR's 2035 targets for climate-impacting emissions is feasible with moderate effort by updating conventional drive systems and optimizing the hydrodynamics of the aft ship. An operational profile was generated through ship monitoring, identifying typical operating points critical for targeted optimization.

The study highlights significant potential for reducing power demand via improved hydrodynamics during aft-ship replacement. Using high-fidelity RANS CFD simulations integrated with a parametric model in an automated optimization environment, the complex hull-propeller-duct interactions in shallow water were accurately modelled. A tailored actuator disk model for ducted propellers and strategic model simplifications enabled an efficient simulation setup, resulting in a 30 % efficiency improvement in shallow water, with additional savings of 16 % and 22 % in deep and moderate water conditions, respectively. The redesigned aft ship features substantial modifications in the transom area, tunnel integration, and frame contour below the tunnel, which primarily influence propeller inflow.

The success of these multi-objective optimizations was validated by preceding model tests, confirming the achieved improvements. This underlines the important role hydrodynamic optimization can play in reducing fossil fuel dependence.

Analysis of the engine load profile revealed that canal navigation imposes unfavourable load conditions on the large engine, while sailing on the Rhine demands significantly more power. This operational insight supports the adoption of a "father-son" dual-engine concept with engines of different sizes, which alone can deliver fuel savings exceeding 5%.

The business case assessment indicates that the key factor for investment payback is the price difference between fossil and renewable fuels. To facilitate adoption, it is crucial to implement subsidy programs to lower upfront costs and to align fuel prices through policies such as fossil fuel sanctions or incentives for renewable alternatives. This combined approach will enhance the economic viability of sustainable propulsion solutions.

The presented results primarily show the potential for optimisation and is based on a rather academic consideration. Further steps must be taken for implementation in order to clarify technical details that were not part of this study. For example, the design of the gearbox for the father-son drive is quite challenging for two motors of such different sizes.

Funded by the Horizon Europe Programme of the European Union under grant agreement No 101096809
Funded by the Horizon Europe guarantee of the United Kingdom, under project No 10068310
Funded by the Swiss State Secretariat for Education, Research and Innovation

1. Introduction

This deliverable describes the evaluation of the concept for the aft ship replacement of the Ernst Kramer. It covers the analysis of the operational profile, hydrodynamic optimisation, model tests and the new engine concept.

The evolution and optimization of vessels ensure their sustained reliability and operational effectiveness. The aft replacement of Ernst Kramer serves as an exemplary case, representing how even a more than 50-year-old vessel can align with contemporary high-level inland vessel design. Retrofitting the aft ship is an extreme task, but it enables the redesign of propulsion arrangements with flex-tunnel, nozzles, and rudders. The optimal choice can result in even more efficient operation with low emissions, minimal fuel consumption, and cost-effectiveness.

Commonly in inland navigation is that the vessels are overpowered, which means operational profile does not require the use of maximum installed power under typical conditions. Nonetheless, for some manoeuvres the power reserve is crucial. Next to the optimization of the hull, it is therefore investigated how engine capacity can be better aligned with actual power demand, with the aim of improving fuel efficiency and reducing emissions.

Funded by the Horizon Europe Programme of the European Union under grant agreement No 101096809
Funded by the Horizon Europe guarantee of the United Kingdom, under project No 10068310
Funded by the Swiss State Secretariat for Education, Research and Innovation

2. Case study – Ernst Kramer

The inland cargo vessel Ernst Kramer was selected as the case study within Work Package 3 of the SYNERGETICS project, focusing on aft-ship replacement. Constructed in 1974 at Arminiuswerft in Bodenwerder, Germany, and currently owned by Rhenus Logistics, the vessel is registered as a dry cargo motor vessel. It is classified as a CEMT Class Va (see [1]), enabling unrestricted navigation along major inland waterways, including the Rhine, Main, and Danube rivers, as well as on connecting canals with appropriate depth and width restrictions.

Over its operational life, the vessel has undergone a series of structural and technical upgrades aimed at enhancing its cargo capacity and performance. In 1985, the vessel was subjected to an extension from 85 up to 105 m (more precisely, 104.97 m), increasing its load capacity from 1822 tons up to 2293 tons. The same year, the bow thruster was added. Subsequent modifications included the retrofit of the side cells in 1993, a propeller duct retrofit in 1995, and the installation of a new main engine in 2004, along with the addition of a car crane.

4 | Main Particulars of demonstration vessel Ernst Kramer.

Length Overall	105 m
Breadth Overall	9.5 m
Depth	4.83 m
Draft Max	3.15 m
Draft Min	0.73 m
Main Engine	Mitsubishi Heavy S16R-MPTA – 1170 kW
Bow Thruster	Verhaar – 315 kW
ENI	04029360

Nowadays, the vessel's propulsion system comprises the aforementioned main engine, Mitsubishi Heavy S16R-MPTA, operating at 1600 RPM, connected via a ZF W 7000 gearbox (reduction ratio 4.127:1) to a 5-blade propeller with a 1.54 m diameter. In addition, a Verhaar bow thruster rated at 315 kW supports manoeuvrability. The vessel's internal cargo space measures 78 m by 7.36 m, and it is equipped with two bow and one stern electric anchor winch. Considering that time, these modifications have contributed to the vessel's ongoing adaptability and efficiency in navigating inland waterways. A summary of the vessel's main particulars is provided in table 4, while Figure 1 shows the vessel in typical operation.

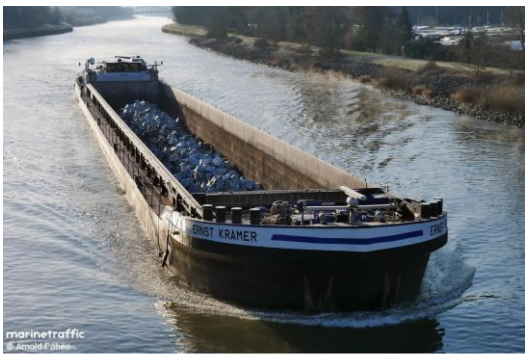

1 | Ernst Kramer during typical inland navigation. The left image - source: MarineTraffic, Arnold P. Dabernig.

Funded by the Horizon Europe Programme of the European Union under grant agreement No 101096809
Funded by the Horizon Europe guarantee of the United Kingdom, under project No 10068310
Funded by the Swiss State Secretariat for Education, Research and Innovation

3. Operational Conditions

To support the aft-ship redesign and other segments of this deliverable, onboard measurements of Ernst Kramer began in mid-April 2022 and are still ongoing. The collected data serves as input for model testing (Chapter 4 and Chapter 6), numerical optimisation (Chapter 5), and the business case assessment (Chapter 7).

To characterise the operational conditions of the vessel, three main parameters were analysed: vessel mean draft, water depth, and vessel speed. All values are presented as time-share distributions within discrete intervals. A broader analysis of other measured parameters follows in subsequent chapters.

The vessel mean draft was evaluated over a range from below 0.7 m to 3.0 m, see figure 2. Trim effects were not included in this analysis. However, it is noted that inland vessels typically operate with a trim angle depending on the sailing direction to reduce grounding risk. The draft interval [0.7–0.8) m accounts for the largest share of total sailing time (22.2 %), followed by [2.4–2.5) m (16.7 %) and [2.5–2.6) m (7.2 %). A bimodal distribution is observed, indicating two dominant loading conditions: lightly laden or empty (draft <1.0 m) and fully laden (draft >2.3 m). Intermediate draft conditions appear significantly less frequently. This confirms that the vessel operates predominantly either empty or at high utilisation.

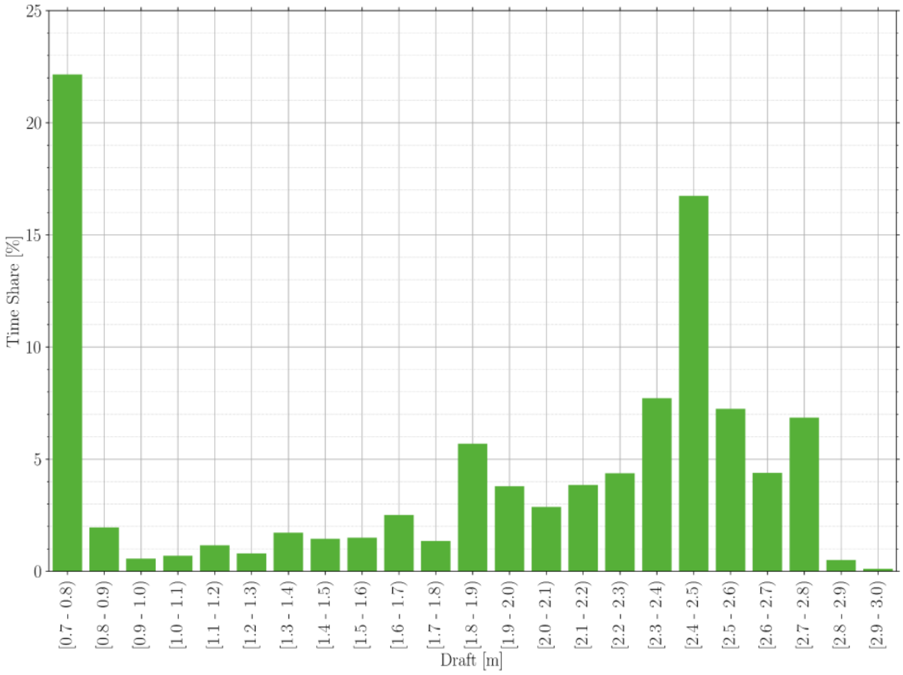

2 | Time-share distribution of vessel mean draft based on onboard measurements.

With respect to water depth, figure 3, the largest share of sailing time (20.8 %) occurred within the [4.0–4.5) m range, followed by [4.5–5.0) m (17.6 %) and [3.5–4.0) m (11.0 %). Over 50 % of sailing time was spent in water depths between 3.5 m and 5.0 m. Less than 5 % of operation occurred in water deeper than 10 m.

The distribution of vessel speed is shown in figure 4, covering an interval from 5 km/h to 25 km/h. The average operational speed was calculated as 12.29 km/h (excluding values less than 5 km/h and above 25 km/h). The most frequent speed range was [10–11) km/h, accounting for 17.5 % of total time, followed by [9–10) km/h (14.3 %) and [11–12) km/h (12.5%). The vessel spent around 50% of the total sailing time at speeds between approximately 9 km/h and 13 km/h. Speeds above 18 km/h are rare (each contributing less than 3 %), indicating that high-speed sailing is limited to exceptional conditions, such as downstream river sections.

Funded by the Horizon Europe Programme of the European Union under grant agreement No 101096809
Funded by the Horizon Europe guarantee of the United Kingdom, under project No 10068310
Funded by the Swiss State Secretariat for Education, Research and Innovation

These operational statistics were used to define representative loading and environmental conditions for model testing and numerical optimisation, as outlined earlier.

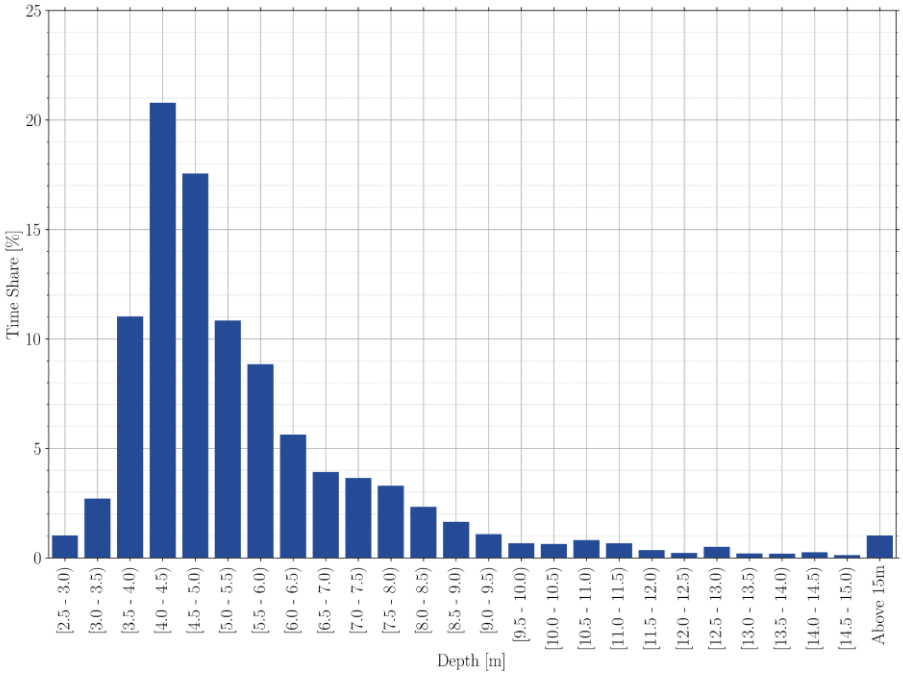

3 | Time-share distribution of water depth based on onboard measurements.

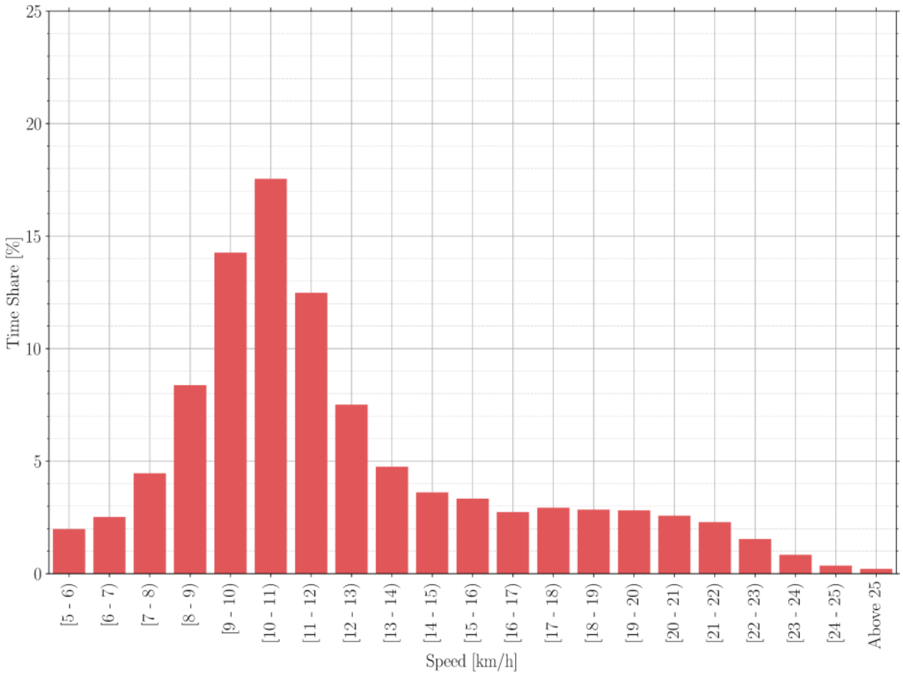

4 | Time-share distribution of vessel speed based on onboard measurements.

Funded by the Horizon Europe Programme of the European Union under grant agreement No 101096809
Funded by the Horizon Europe guarantee of the United Kingdom, under project No 10068310
Funded by the Swiss State Secretariat for Education, Research and Innovation

According to ITTC (2017a) [2], shallow water effects on ship resistance should be considered when at least one of the following conditions is met:

- $\frac{h}{T} < 4$, or
- $Fr_h > 0.5$, where $Fr_h = V/\sqrt{g \cdot h}$ is the Froude depth number.

To assess how frequently the vessel operates under shallow water conditions, two scatter plots were generated from the onboard dataset. The dataset includes only sailing points within the following bounds: vessel speed (V) between 5 and 25 km/h, water depth (h) between 2 and 20 m, and mean draft (T) 0.7 and 3 m. Figure 5 presents the ratio $\frac{h}{T}$ against measured water depth and corresponding vessel mean draft. Data points where $\frac{h}{T} < 4$ are highlighted in orange, indicating geometrical shallow water conditions. Figure 6 shows vessel speed against water depth, with colored points based on the Froude depth number Fr_h. Data points where $Fr_h > 0.5$ are highlighted in orange, indicating dynamic shallow water conditions.

Both indicators confirm, clear visual separation between two domains, that the vessel regularly operates under shallow water conditions according to ITTC guidelines. Quantitatively, the condition $Fr_h > 0.5$ was met in 33.26 % of the measured data, while $\frac{h}{T} < 4$ occurred in 79.15 % of the cases. The findings indicate that dynamic shallow water effects are occasional and linked to specific conditions, whereas geometrical shallow water conditions are common throughout operations. Accordingly, both effects must be considered in all subsequent analyses.

Funded by the Horizon Europe Programme of the European Union under grant agreement No 101096809
Funded by the Horizon Europe guarantee of the United Kingdom, under project No 10068310
Funded by the Swiss State Secretariat for Education, Research and Innovation

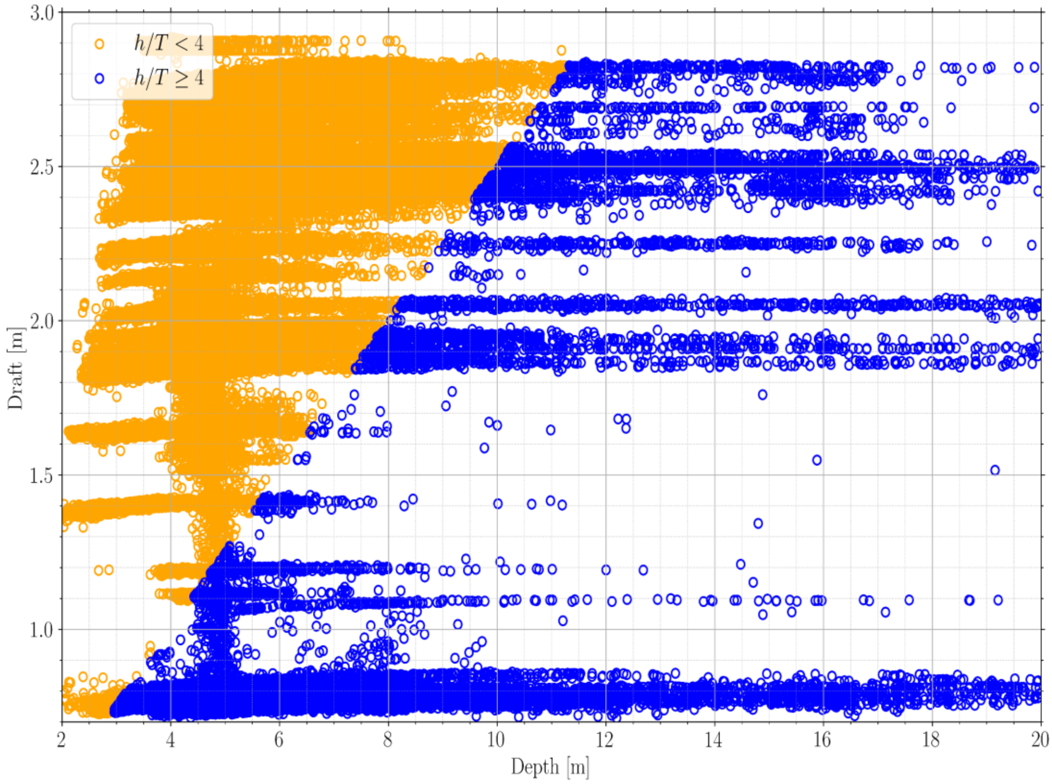

5 | Shallow water effect based on the depth-to-draft ratio. Orange: $\frac{h}{T} < 4$ (shallow water), blue: $\frac{h}{T} \geq 4$. Data filtered: $5 \leq V \leq 25\ km/h$, $2 \leq h \leq 20\ m$, and $0.7 \leq T \leq 3\ m$.

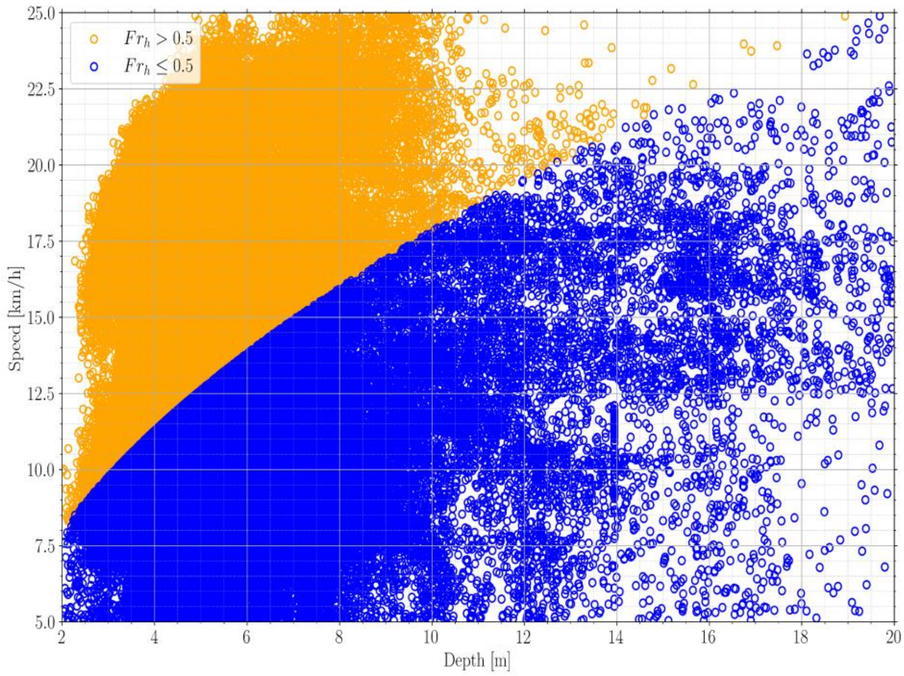

6 | Shallow water effect depth Froude number. Orange: $Fr_h > 0.5$ (shallow water), blue: $Fr_h \leq 0.5$ Data filtered: $5 \leq V \leq 25\ km/h$, $2 \leq h \leq 20\ m$, and $0.7 \leq T \leq 3\ m$

Funded by the Horizon Europe Programme of the European Union under grant agreement No 101096809
Funded by the Horizon Europe guarantee of the United Kingdom, under project No 10068310
Funded by the Swiss State Secretariat for Education, Research and Innovation

4. Model tests

4.1 Facilities

In order to evaluate the hydrodynamic performance of the vessel Ernst Kramer and assess the effects of a modified aft-body, a dedicated model test campaign was carried out at the Development Centre for Ship Technology and Transport Systems (DST) in Duisburg, Germany. The objective was to obtain experimental data under realistic operating conditions (as described in the previous chapter), to serve both as a baseline for subsequent CFD validation and optimisation, and as a reference for direct comparison with the optimised hull form.

The experiments took place in the large shallow water towing tank (see figure 7), featuring a total length of 200 m, width of 10 m, and adjustable water depth up to 1.2 m. The facility is specifically designed to replicate shallow and confined water conditions typical for inland navigation, allowing detailed investigation of depth-dependent hydrodynamic effects.

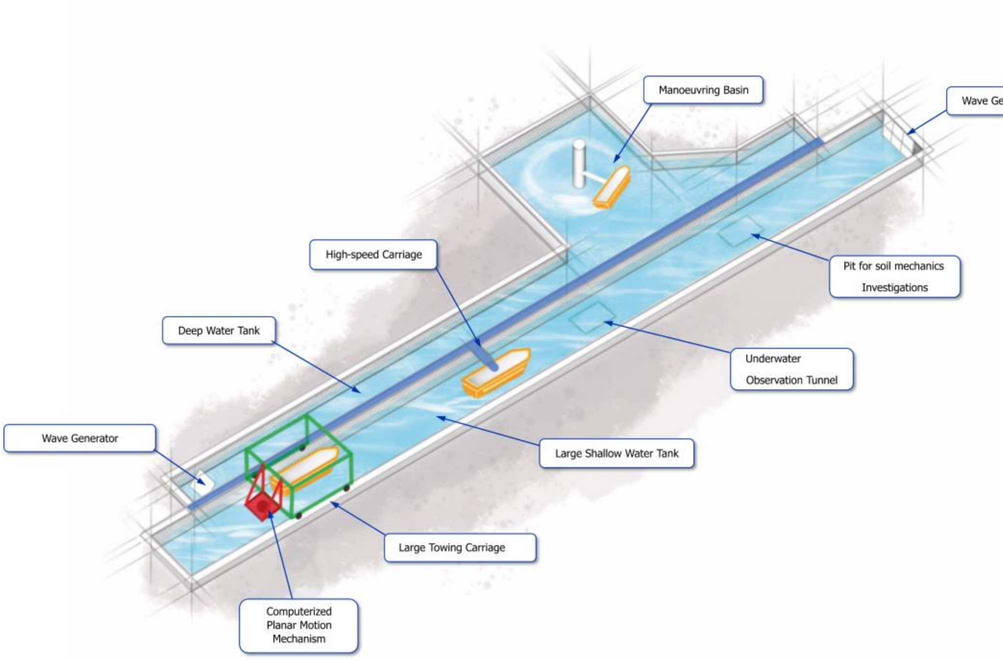

7 | Layout of the facilities at Development Centre for Ship Technology and Transport Systems (DST) in Duisburg, Germany.

A unique feature of this basin is the observation tunnel located directly beneath the towing track, equipped with 60 mm thick acrylic windows, allowing for underwater flow visualization during test runs. The towing carriage provides high-precision control of model speed and is equipped with calibrated instrumentation for measuring towing force, shaft torque, thrust, trim, sinkage, and other relevant parameters. Although DST's facilities support a wide range of additional testing capabilities, including wave generation, manoeuvring tests, and advanced flow diagnostics, these were not employed in the present study, which focused exclusively resistance and propulsion measurements. For full-scale performance prediction, both tests were carried out in accordance with the International Towing Tank Conference (ITTC) Recommended Procedures. Importantly, the same facility and testing methodology were later applied to the optimised aft-ship configuration without modification, ensuring consistency and comparability between both designs.

Funded by the Horizon Europe Programme of the European Union under grant agreement No 101096809
Funded by the Horizon Europe guarantee of the United Kingdom, under project No 10068310
Funded by the Swiss State Secretariat for Education, Research and Innovation

4.2 Model production

The physical model of Ernst Kramer was manufactured at DST (see figure 8) to a geometric scale of 1:12.1, using traditional wooden construction. The model with initial aft design, referred to as M2202, was designed in two main sections: a fixed bow and midship, and an interchangeable aft-ship module. This modular design enabled testing of different aft-ship geometries under identical conditions. The same bow and midship sections were later reused for the model with the optimised stern (M2211), ensuring full comparability between both configurations.

Both variants were equipped with a single ducted propeller, and a fixed two rudders. No active rudder deflection was applied during the tests. Flow visualization was supported by attaching woollen threads at selected locations on the model's stern, and underwater video recordings were made while passing the observation tunnel.

8 | Manufacturing process of the original model geometry (M2202) at DST premises.

A conventional set of three model tests was used to investigate the interaction between the hull and the propulsion system:

- Open water test,
- Resistance test, and
- Self-propulsion test.

In the open water test, the characteristics of the propulsion system are determined under uniform inflow conditions. Since a propulsor with previously known performance characteristics was used, this test was not repeated in the current campaign. The resistance test, performed with the bare hull configuration (i.e., without propeller and rudders), provided insights into the vessel's hydrodynamic drag. The self-propulsion test was carried out according to the British method, using three different propeller rotational speeds per towing speed to establish the self-propulsion point.

The same testing methodology and model configuration were consistently applied to the optimised aft-ship, ensuring a reliable basis for comparison between both designs.

Funded by the Horizon Europe Programme of the European Union under grant agreement No 101096809
Funded by the Horizon Europe guarantee of the United Kingdom, under project No 10068310
Funded by the Swiss State Secretariat for Education, Research and Innovation

4.3 Test campaign with baseline model

Based on the operational conditions outlined in Chapter 3, the test campaign, summarised in table 5, included model-scale resistance and propulsion tests at speeds ranging from 10 km/h to 18 km/h. The selected conditions were chosen to reflect the most representative operational states of the vessel, taking into account under keel clearance and the corresponding depth Froude number. For the water depth 3.5 m only the lowest two velocities were tested, as the vessels do not sail faster in these shallow water conditions.

The draught conditions were defined based on the observed bimodal distribution of mean draft (see figure 2), which revealed that the vessel predominantly operates either fully laden (draft > 2.3 m) or lightly laden/empty (draft < 1.0 m), with intermediate loading occurring less frequently. Accordingly, three representative loading conditions were selected: full load (T = 2.8 m), partial load (T = 1.9 m), and a light ship condition with trim by stern (T_A = 1.35 m, T_F = 0.75m).

Water depths of 7.5 m, 5.0 m, and 3.5 m were selected to represent deep, intermediate, and shallow conditions, in line with the time-share distribution shown in figure 3, where over 50 % of sailing time occurs in depths between 3.5 m and 5.0 m. Depths above 7.5 m, while less frequent, were included to establish a deep-water baseline.

Test speeds were aligned with the vessel's typical operational profile (figure 4), with about 50% of the sailing time spent at speeds between 9 km/h and 13 km/h, while maximum speeds rarely exceeded 18 km/h.

5 | Overview of test campaign parameters in the full scale.

↓ T [m] / h [m] →	$h = 7.5\,m$	$h = 5\,m$	$3.5\,m$
LC1 $T_A = 2.8\,m\,;T_F = 2.8\,m$	$V_1 = 12\,km/h$ $V_2 = 16\,km/h$ $V_3 = 18\,km/h$	$V_1 = 12\,km/h$ $V_2 = 16\,km/h$ $V_3 = 17\,km/h$	$V_1 = 10\,km/h$ $V_2 = 12\,km/h$
LC2 $T_A = 1.9\,m\,;T_F = 1.9\,m$	$V_1 = 12\,km/h$ $V_2 = 16\,km/h$ $V_3 = 18\,km/h$	$V_1 = 12\,km/h$ $V_2 = 16\,km/h$ $V_3 = 17\,km/h$	$V_1 = 10\,km/h$ $V_2 = 12\,km/h$
LC3 $T_A = 1.35\,m\,;T_F = 0.75\,m$	$V_1 = 12\,km/h$ $V_2 = 16\,km/h$ $V_3 = 18\,km/h$	$V_1 = 12\,km/h$ $V_2 = 16\,km/h$ $V_3 = 17\,km/h$	$V_1 = 10\,km/h$ $V_2 = 12\,km/h$

LC - Loading Condition; T_A - draught at aft perpendicular; T_F - draught at forward perpendicular; h – water depth; v - speed

Figure 9 illustrates the results obtained for the original aft-ship configuration (denoted as M2202) which reveal a marked sensitivity to water depth, vessel speed, and loading condition. As expected, the delivered power required for propulsion increased with both vessel speed and draught, with the most pronounced shallow water effects observed at h = 3.5 m across all load cases.

In Loading Condition 1 (LC1) - full load (T = 2.8 m) - shallow water has the strongest impact. For example, at 12 km/h, the delivered power increases by nearly 48% when comparing deep water (h = 7.5 m) to shallow water (h = 3.5 m). The effect becomes even more pronounced at higher speeds. LC2, representing partial load (T = 1.9 m), follows the same trend, with a moderate increase of about 10% in delivered power at 12 km/h between deep and shallow water. In LC3, simulating an empty vessel with trim by stern (TA = 1.35 m, TF = 0.75 m), the shallow water effect is smallest, but still noticeable - for instance, at 12 km/h, power demand rises by around 5% when moving from deep to shallow water.

Funded by the Horizon Europe Programme of the European Union under grant agreement No 101096809
Funded by the Horizon Europe guarantee of the United Kingdom, under project No 10068310
Funded by the Swiss State Secretariat for Education, Research and Innovation

These findings confirm the combined influence of water depth and loading condition on propulsion demand, as the power increase in shallow water is known to be a consequence of the interaction between the (viscous) flow around the ship and the riverbed. This interaction is most notable at the stern, therefore the optimization efforts, described in chapter 5, focus on the stern region of the vessel

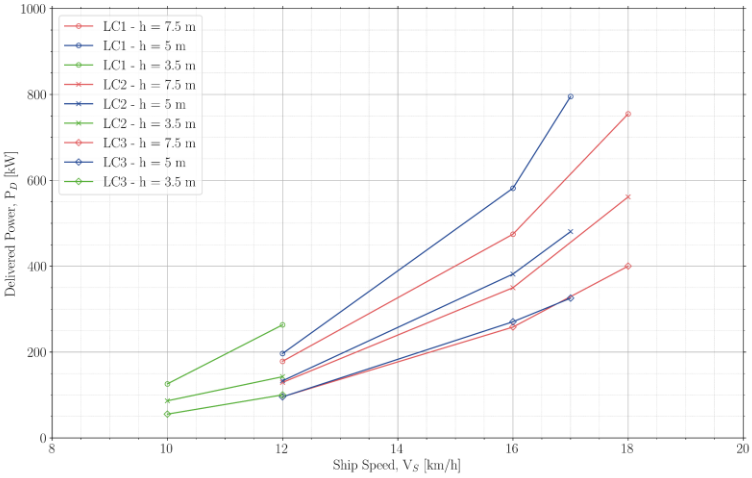

9 | Predicted power demand in the full scale for the original design (M2202) across various loading conditions, water depths, and vessel speeds.

Funded by the Horizon Europe Programme of the European Union under grant agreement No 101096809
Funded by the Horizon Europe guarantee of the United Kingdom, under project No 10068310
Funded by the Swiss State Secretariat for Education, Research and Innovation

5. Multi-objective Optimisation

A multi-objective global optimisation based on a two-step approach was used to find an optimised design with respect to minimum power demand when operating in confined waters. The selected approach consists of a design space exploration followed by a response surface optimisation to determine the best combination of the selected design variables.

5.1 Design Conditions

As shown in Chapter Operational Conditions3 describing the onboard measurements and data analysis, the use case vessel operates in tramp service on various waterways with different boundary conditions and free-flowing rivers with significant fluctuations of water level. To cover the relevant bandwidth for the optimisation representative conditions in terms of water depth and corresponding speeds were identified the two design conditions DC2 and DC3 shown in table 6 were judged to be representative for the gain in power in operational conditions and thus selected as objective for the latter multi-objective optimization. The DC1 conditions was selected as an additional case for the validation study.

6 | Selected design conditions for the CFD study

ID	Draft	Depth	Ship Speed	h/T	Fr_h	Condition
-	T	h	V_S	-	-	-
DC1	2.8 m	7.5 m	16 km/h	2.7	0.518	Deep
DC2	2.8 m	5.0 m	16 km/h	1.8	0.635	Intermediate
DC3	2.8 m	3.5 m	12 km/h	1.25	0.569	Shallow

5.2 Numerical Method and Simulation Setup

5.2.1 Flow Solver

General

All CFD simulation results were performed with the open-source CFD software library OpenFOAM[1]. The used flow solver interFoam solves the Reynolds-Averaged Navier-Stokes (RANS) equations using a finite volume method (FVM) for two incompressible, isothermal, and immiscible fluids employing the Volume of Fluid (VoF) method. Pressure-velocity coupling is done with the PIMPLE approach, a hybrid scheme that combines the PISO (Pressure-Implicit Split Operator) and SIMPLE (Semi-Implicit Method for Pressure-Linked Equations) algorithms [3]. An additional phase-fraction transport equation tracks the interface between the two fluids. To ensure mass conservation whilst keeping the interface sharp, interFoam relies on the MULES (Multidimensional Universal Limiter for Explicit Solution [4]) method for the VoF transport equation. For the turbulence closure of the RANS equations the two-equation linear eddy viscosity model k-ω SST model [5] was selected. This model has shown to perform well in the field of ship resistance and propulsion applications and is able to predict the complex flow including separations at ship aft bodies under shallow water conditions in various studies [6].

[1] https://openfoam.org/versions/dev

Funded by the Horizon Europe Programme of the European Union under grant agreement No 101096809
Funded by the Horizon Europe guarantee of the United Kingdom, under project No 10068310
Funded by the Swiss State Secretariat for Education, Research and Innovation

Body Dynamics and Mesh Motion

To account for the ship’s dynamic position, OpenFOAM provides a library to calculate motion of a discrete number of articulated rigid bodies. The resulting mesh motion caused by the body motions is accomplished by interpolation using septernion averaging. The mesh points are moved with a SLERP (spherical linear) interpolation of the movement as a function of distance to the object surface. Points near the moving object (the ship) move according to the motion state of the ship (translations and rotations), while the motion of the points in the far-field are scaled, based on their distances from the ship’s hull. Far away from the hull, the mesh points are fixed, thus the initial grid topology (including the refinement regions) is not changed. This method is computationally very efficient and can accommodate relatively large body motions efficiently.

Propulsion

The propeller was not geometrically modelled. Instead, an Actuator Disk method was used, mimicking the effect of the propeller by accelerating the fluid with the help of volumetric body forces. The model is a DST in-house implementation, described comprehensively in [7]. To note the most important features, the model:

(1) calculates the self-propulsion point iteratively
(2) accounts for user-defined open water characteristic
(3) determines the actual propeller inflow by correcting the current flow field due to the propeller and duct induced thrust with a momentum-theory based approach and
(4) radially distributes the normal and tangential forces, tailored for ducted propellers.

5.2.2 Simulations

General

Comprehensive experimental data was available for the use case vessel. Thus, all simulations have been done in model scale with a scaling factor of 12.1. To ensure consistent results the computational domain’s lateral dimension was set according to the breadth of DST’s towing tank of 9.8 m. The inlet and outlet boundaries were located 2.5 times and 4 times the ship lengths in front and behind the ship, respectively. The bottom’s position was given by the investigated water depth. Both dynamic trim and sinkage were considered to determine the correct floating position, while all other degrees of freedom were supressed (2DoF).

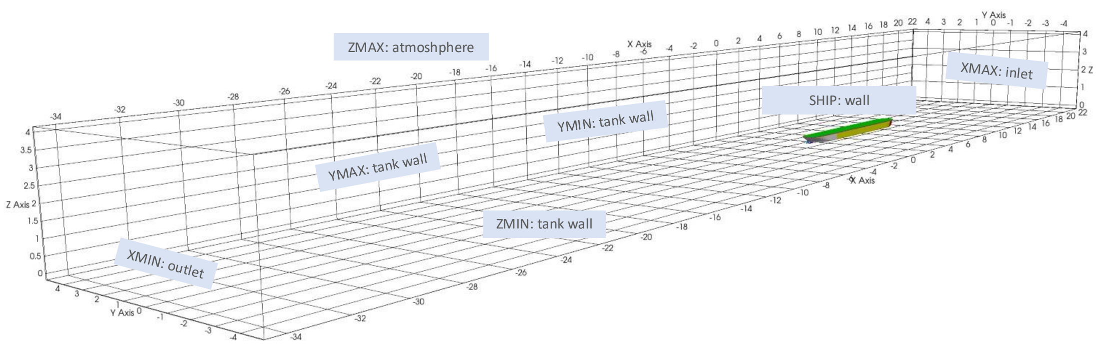

10 | Sketch of the computational domain and boundary conditions as used in the CFD simulations

Funded by the Horizon Europe Programme of the European Union under grant agreement No 101096809
Funded by the Horizon Europe guarantee of the United Kingdom, under project No 10068310
Funded by the Swiss State Secretariat for Education, Research and Innovation

Boundary and initial conditions

At the inlet the ship’s forward speed, water level and turbulent quantities were prescribed. The turbulence quantities were calculated under the assumption of a low turbulence level, i.e. the turbulence intensity Tu of 10 % and the viscosity ratio μt/μ of 10. Downstream at the outlet a mixed Dirichlet-Neuman condition was used which ensures correct mass flow and keeps the water at correct level. The interaction between hull and waterway bottom due to the small distance in case of shallow water requires careful selection of the bottom and side boundaries. A no-slip condition with wall functions was used with a prescribed tangential velocity according to the ship’s speed to account for the correct relative velocity between ship and tank walls. On the hull surface also a no-slip condition was used with a wall function, which relies on Spalding’s law to give a continuous profile of the viscous sublayer [8]. To avoid strong disturbances the velocity field is not initialized with the ship speed but instead is ramped from zero to full speed. With decreasing water depth, the ramping duration needs to be increased. That effect can be estimated by scaling the ramp duration with

$$c_{Ramp} = 10e^{-1.1\frac{h}{T}} + 1$$

where h is the water depth and T the ship draft. The ramp needs to be applied not only at the boundaries, but also in the domain by applying additional body forces to accelerate the fluid. This procedure avoids strong oscillations and thus helps to reduce the simulation time significantly.

Meshing

The unstructured polyhedral meshes generated with OpenFOAM’s tool snappyHexMesh consist of hexahedral cells and so-called prism layers near surfaces. An example snapshot is shown in figure 11. The overall refinement topology and cell sizes follow in-house best practice settings and can be summarised as follows: a base cell size is defined as fraction of the ship length. Isotropic refinements in regions with high gradients and at surfaces with strong curvatures such as bow and stern section, wake region and at appendages like ducts, shafts and rudders are specified by defined refinement levels. E.g. for the mesh around the duct the base cells are split 8-9 times to resolve the geometry properly and predict the flow accurately. Away from the hull the cells are smoothly stretched in the horizontal plane. To ensure a shape interface between air and water, the cells are refined in vertical direction. All generated meshes consisted of around 5 million cells in total.

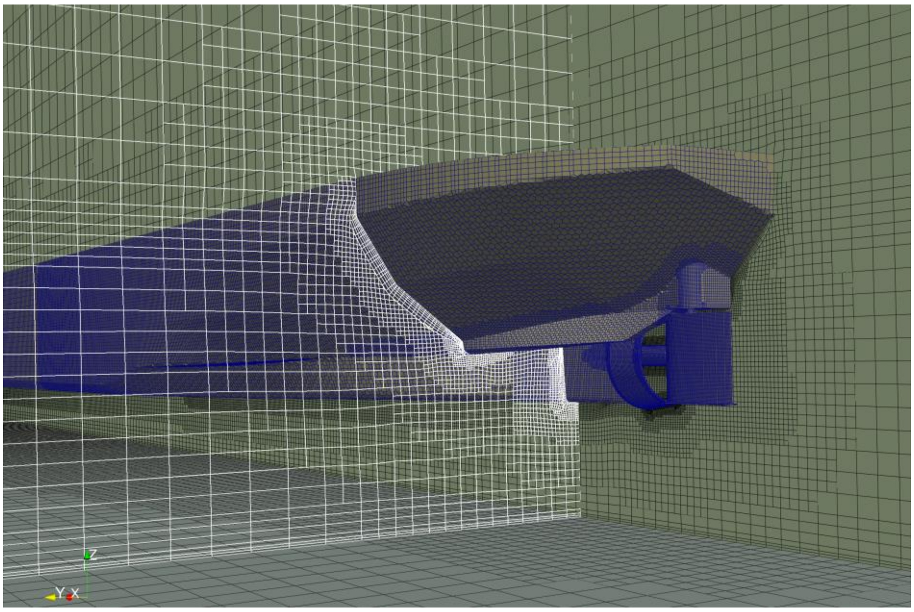

11 | Mesh example in the aft ship region with transversal cut (white grid lines), bottom boundary and longitudinal cut at centre plane.

Funded by the Horizon Europe Programme of the European Union under grant agreement No 101096809
Funded by the Horizon Europe guarantee of the United Kingdom, under project No 10068310
Funded by the Swiss State Secretariat for Education, Research and Innovation

Numerical schemes

The momentum transport is discretised with a second order linear upwind scheme. A first order upwind scheme was used for the turbulence equations. Only time averaged integral quantities were of interest, thus temporal discretisation was done with a first order Euler time scheme. Robust but accurate gradient calculation was ensured with a selective cubic limiter [9].

5.3 Case Study

5.3.1 Validation

In a first step the CFD setup was verified by comparing the simulation results with the experiments. The graphs in figure 12 show the predicted full-scale delivered power curves from experiments for various combinations of ship speeds and water depths.

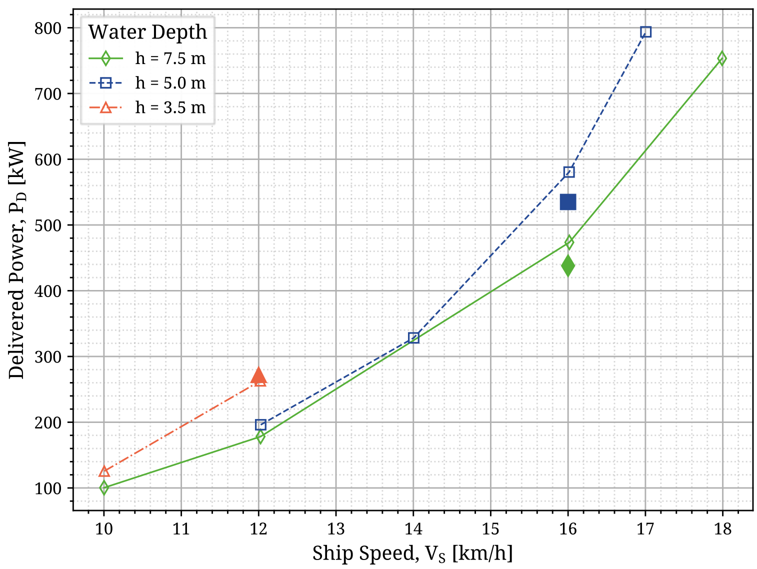

12 | Comparison of predicted delivered power PD from experiments (empty markers) and simulations (filled markers)

Filled markers represent the CFD results and the empty markers the EFD results, respectively. In general, the numerically predicted delivered power values P_D show a good agreement with the experiments. For the shallow water case (h = 3.5 m, T = 2.8 m, and V_S = 12 km/h), the difference is just around 3.5 %. For the intermediate and deep-water case (DC2 and DC3) the CFD calculated P_D is approx. 8 % lower, which is still quite satisfactory keeping in mind the complex flow of ducted propellers. The strong interaction between hull resistance, wake fraction, thrust deduction, and propeller- and duct thrust makes the prediction of the self-propulsion point very sensitive to small differences. Besides for the optimization it is more important to predict the trends due to geometrical variation instead of the absolute values.

Figure 13 shows an example of the longitudinal forces calculated in the CFD simulations. The graphs show the development over time for the pressure, viscous and total (sum of pressure and viscous) components. The grey area from 0 to 30 s marks the velocity ramping phase (as described in the previous chapter), while the area from 92 to 122 s corresponds to the final simulation phase with an adjusted time step to ensure valid Courant number.

Funded by the Horizon Europe Programme of the European Union under grant agreement No 101096809
Funded by the Horizon Europe guarantee of the United Kingdom, under project No 10068310
Funded by the Swiss State Secretariat for Education, Research and Innovation

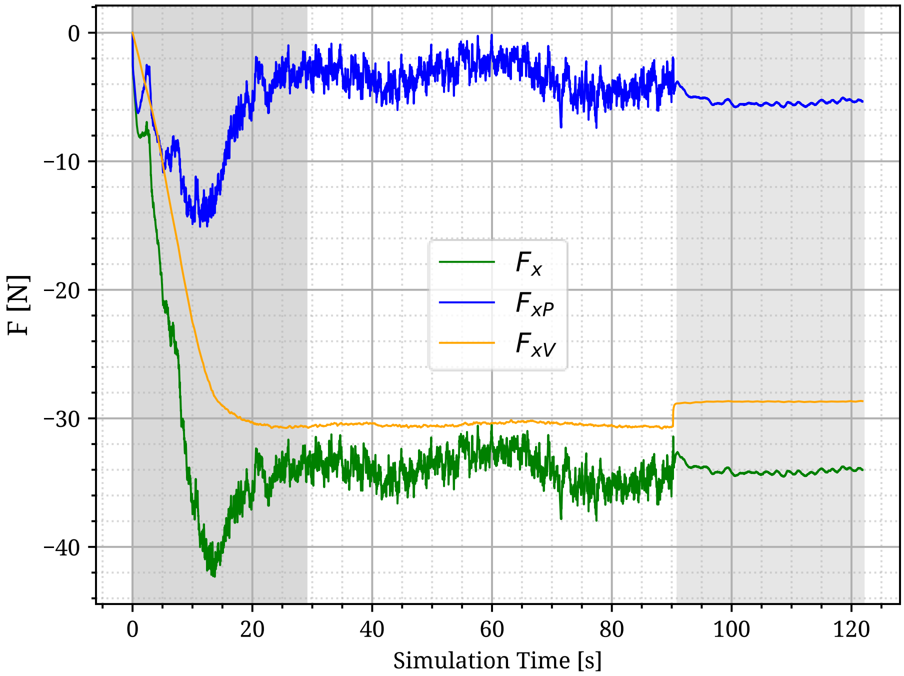

13 | Example time series from the CFD propulsion simulations

The following figures compare the wave pattern and the velocity distribution for the three simulated cases. The dependency on the water depth can be clearly seen in both the wave field and the velocities. For clarity the free surface elevation is scale to full scale and the scalar bar range is same for all three cases, while for the velocity distribution the maximum value of the scalar bar is set to 1.25 times the ship speed.

Funded by the Horizon Europe Programme of the European Union under grant agreement No 101096809
Funded by the Horizon Europe guarantee of the United Kingdom, under project No 10068310
Funded by the Swiss State Secretariat for Education, Research and Innovation

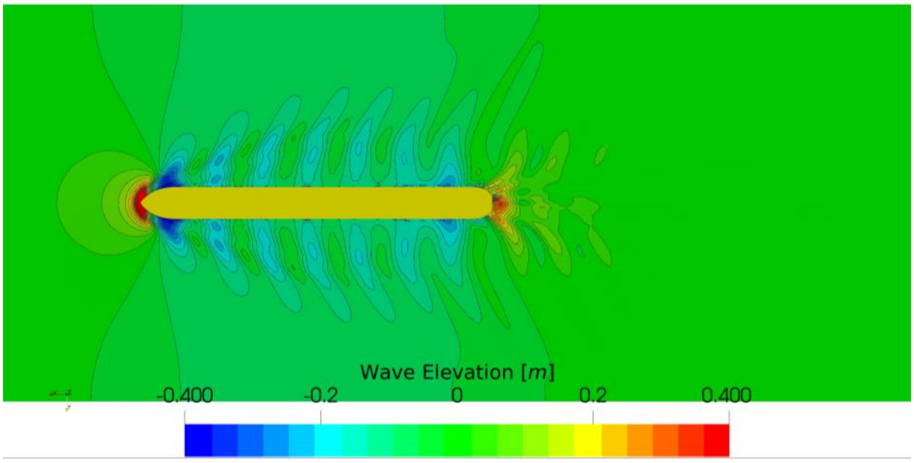

DC1: V_S = 16 km/h, h = 7.5 m

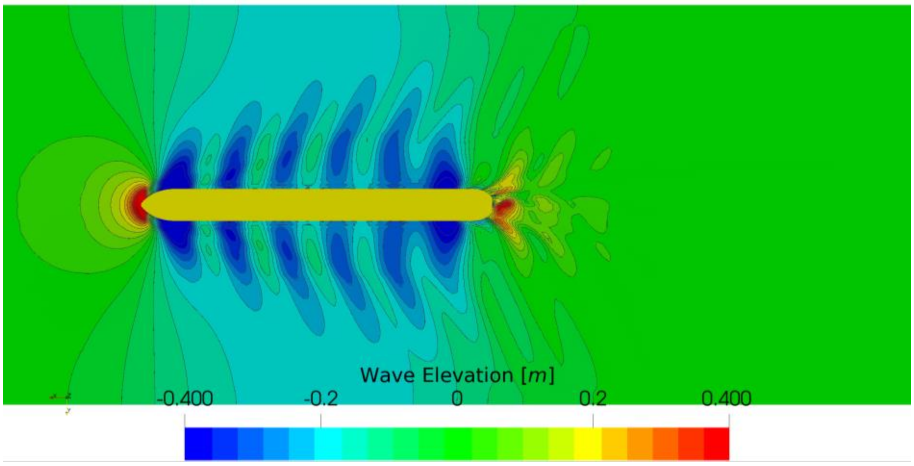

DC2: VS = 16 km/h, h = 5.0 m

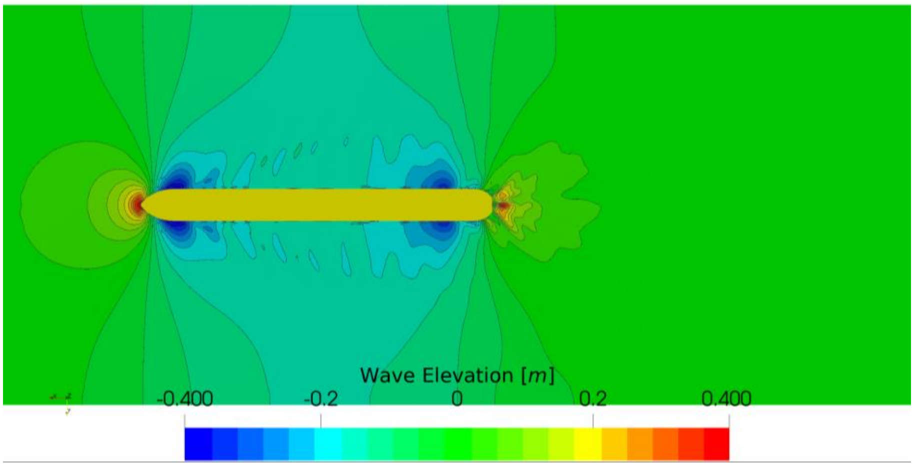

DC3: VS = 12 km/h, h = 3.5 m

14 | Free surface elevation (scaled to full scale).

Funded by the Horizon Europe Programme of the European Union under grant agreement No 101096809
Funded by the Horizon Europe guarantee of the United Kingdom, under project No 10068310
Funded by the Swiss State Secretariat for Education, Research and Innovation

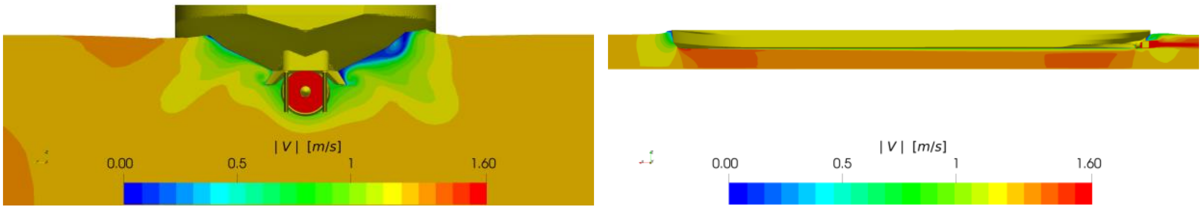

DC1: V_S = 16 km/h, h = 7.5 m

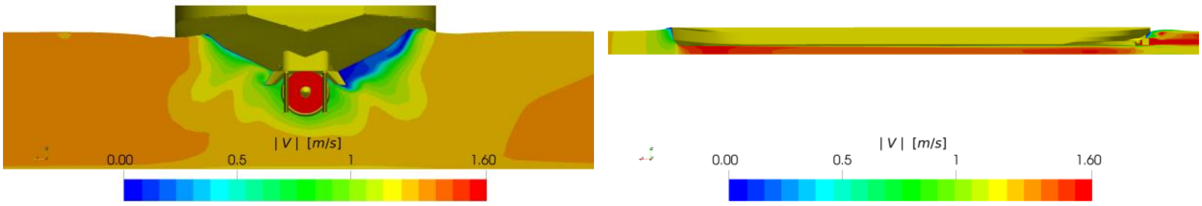

DC2: VS = 16 km/h, h = 5.0 m

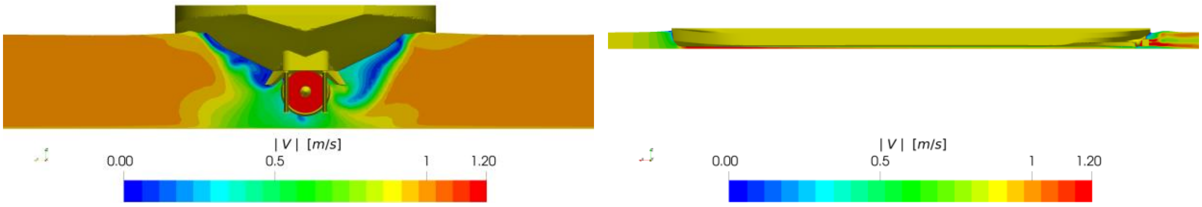

DC2: VS = 12 km/h, h = 3.5 m

15 | Velocity distribution at the propeller- (left) and center-plane (right); maximum value of scalar range corresponds to 1.25 times V_S

Funded by the Horizon Europe Programme of the European Union under grant agreement No 101096809
Funded by the Horizon Europe guarantee of the United Kingdom, under project No 10068310
Funded by the Swiss State Secretariat for Education, Research and Innovation

5.4 Re-Design

Design specifications

Different design constraints were given for the replacement study of the complete aft-ship. The overall main dimensions such as length over all and moulded breadth should not be changed. Besides, either the maximum (3.2 m) and design draft (2.8 m) should be same, and operation at a minimum draft of 1.3 m needs to be ensured. The demand to minimize the effort of reconstruction, the position of the engine room bulkhead was fixed, i.e. both the length of the aft ship and the length of the parallel midship section are clearly defined. Finally, it was decided to keep same propulsion configuration, i.e. a single propeller with same diameter of 1.6 m. Important design aspect for a cargo vessel relates to the loading capacity. For this study a small reduction of a maximum of 30 tonnes of the loading capacity was allowed.

New conceptual designs

Two new aft-ship variants have been designed based on the above-described specifications. Figure 16 shows the original aft ship on the left and the two new concepts in the middle and right, resp. These new variants are referred to as SYN1 and SYN2 in the rest of the document. While SYN1 follows the original hull lines, but avoids the very sharp edges of the original design, SYN2 shows a much smoother characteristics by using S-shaped frames below the tunnel. Besides, the transom regions differ significantly. The lower edge of the relatively small, tri-angular shaped transom of SYN1 is above the undisturbed waterline at the design draft of 2.8 m, i.e. the transom will not or only marginally be submerged. In contrast, SYN2 has a much larger transom area with a lower edge below the design draft.

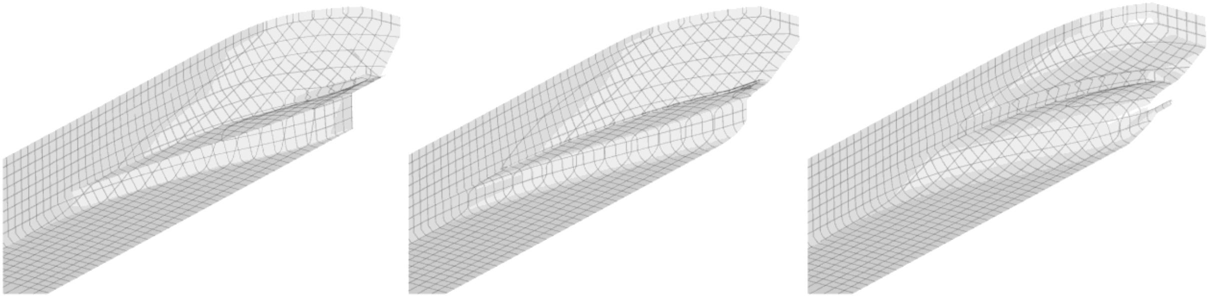

16 | Illustration of the different aft ship designs : Original MV Ernst Kramer (left), new concept SYN1 (middle) and SYN2 (right)

Baseline performance

Prior to the actual optimization, the baselines of the two newly designed variants SYN1 and SYN2 were simulated for the three selected design conditions and compared to the CFD results of the original Ernst Kramer. The predicted PD values are given in table 7 as relative difference to Ernst Kramer. For all three conditions both designs outperform the original hull. At deep and intermediate condition, the gain is similar for both SYN1 and SYN2. For the shallow water case the predicted power demand reduction of SYN1 is around just 4 %, while even without any optimization the concept of SYN2 shows a significant improvement of approx. 28 % compared to Ernst Kramer design.

Funded by the Horizon Europe Programme of the European Union under grant agreement No 101096809
Funded by the Horizon Europe guarantee of the United Kingdom, under project No 10068310
Funded by the Swiss State Secretariat for Education, Research and Innovation

7 | Comparison of the performance of the new concepts to the original Ernst Kramer

Design Condition	SYN1 – Baseline	SYN2 – Baseline
DC1 (deep)	-14 %	-14 %
DC2 (intermediate)	-9 %	-9 %
DC3 (shallow)	-4 %	-28 %

Figure 17 shows the pressure (c_p) and friction (c_f) distribution in the aft-ship region of all the variants for condition DC1. Especially the lower pressure gradient of both new designs due to smoother hull lines can be clearly seen. Furthermore, the different transom designs SYN1 and SYN2 strongly influence the flow separation (blue areas in the c_f distribution) behaviour: For SYN1 there is a relatively large area above the propeller, while most of the separation occurs at the submerged transom of SYN2. Despite the quite different distributions both variants show very similar P_D values for this condition.

Even though SYN1 has not shown such significant improvement for the shallow water condition, both variants were investigated in a subsequent optimization study to identify possible improvements and derive insights in the most relevant parameters for efficient shallow water designs.

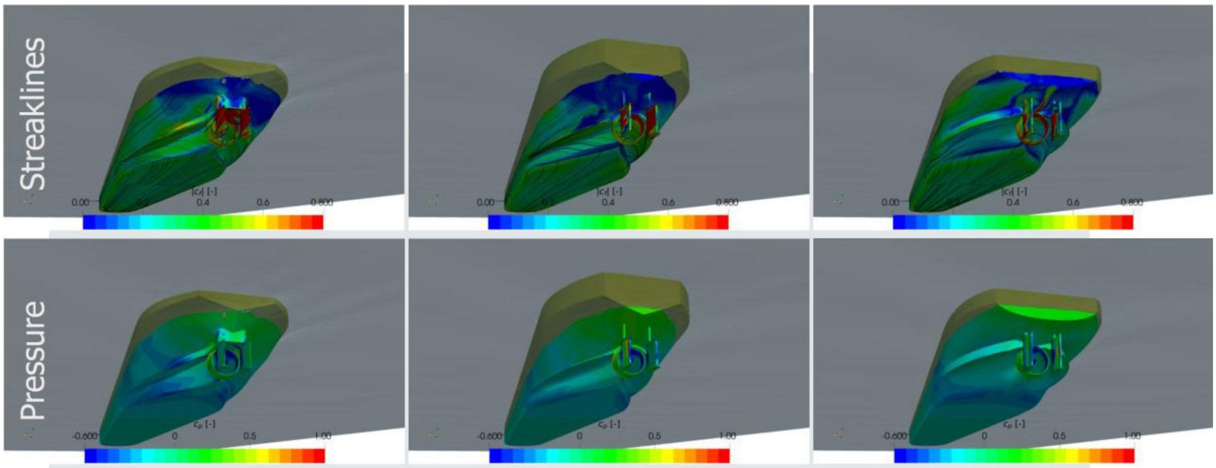

17 | Comparison of friction (top) and Pressure (bottom) distribution for Ernst Kramer (left), SYN1 (middle) and SYN2 (right) variants

Funded by the Horizon Europe Programme of the European Union under grant agreement No 101096809
Funded by the Horizon Europe guarantee of the United Kingdom, under project No 10068310
Funded by the Swiss State Secretariat for Education, Research and Innovation

5.5 Optimization

5.5.1 Methodology

The design study of both variants was done with the software CAESES. With the integrated software connector DST's fully scripted CFD environment for meshing and simulation was coupled with the automated CAD engine and optimization algorithms of CAESES.

Minimizing the required PD for the two design conditions DC2 (intermediate) and DC3 (shallow) was defined as objective for the optimization. The lowest allowed displacement was constrained to 2460 t, corresponding to a slightly reduced dis-placement by max. 30 t (1.6 %) compared to the original Ernst Kramer. During the simulations besides the propulsion power also the required thrust was monitored, both in absolute and specific (per tonnage) values. The optimization itself was done in two consecutive steps: first a design space exploration (DSE) was performed, i.e. with a quasi-random distribution (SOBOL) of the design variables the dependency of the design variables on the objective was investigated. Based on the DSE results a surrogate model was trained using a response surface (RS) approach. This RS was used then to minimize the propulsion power for both design conditions.

To ensure a global minimum is found, some hundred different designs need to be simulated. Even with the efficient CFD setup described in chapter 5.2.2 the computational effort is still too high. Thus, instead of time-resolved free surface simulations the double-body method was used. By replacing the free surface with a symmetry plane and a steady-state time scheme, the computational effort is reduced significantly, almost by a factor of hundred. This approach has been proven to perform well recently, and was improved here by accounting for an approximated dynamic floating position. Values for trim and sinkage were taken from the free surface simulations of the baseline performance study for the corresponding condition. The CAD model of each generated design during the optimization was then transformed (translated in vertical direction and rotated around the transverse axis) prior to the meshing process.

5.5.2 Parametric Model

Using CAD models in an automated, streamlined optimization process requires a parametrized model. This enables robust design variations without the need to re-build the entire model manually. In general, a 3D model is parametrized by defining key parameters such as dimensions, angles, and features that allow to adjusted the geometry either locally or globally. In this study, the CAE software CAESES was used to generate the parametrized CAD models. In principle, CAESES offers two methods: fully- and partially-parametric modelling. The partially-parametric model-ling, e.g. RBF morphing, is relatively simple to set-up, but is in turn to some extent limited in the amount of geometrical variation. The partially-parametric modelling approach works as follows: a certain area of an existing NURBS geometry is selected, where a deformation of the geometry is allowed. Features (points, curves, or surfaces) on that area are defined as sources and transformed versions of those features, e.g. offset of the source feature, are set as targets. Source to target mapping controls the deformation. In contrast, a fully-parametric model builds the geometry from scratch, which adds more flexibility and allows for much larger and more specific variation. Depending on the complexity of the model, this can cover not only local modifications but also the variation of the main dimensions.

Funded by the Horizon Europe Programme of the European Union under grant agreement No 101096809
Funded by the Horizon Europe guarantee of the United Kingdom, under project No 10068310
Funded by the Swiss State Secretariat for Education, Research and Innovation

SYN1: Partially-parametric model

For the SYN1 variant the parametric model was created based on the above-described morphing technique: the surfaces below the tunnel were selected for deformation, cyan coloured in figure 18. Two intersection curves, C_{up} and C_{low} in the upper- and lower-part resp., define the transformation sources (the green curves). The transformation target curves are generated by offsetting these curves with parametrized offset factors. These factors are controlled by specifying the horizontal shift of points on theses curves, one each in the fore and aft part ($P_{up,fore}$, $P_{up,aft}$ and $P_{low,fore}$ and $P_{low,aft}$, resp. With one additional point $P_{low,mid}$, controlling the vertical offset of the lower curve, a total of 5 design variables controls this relatively simple parametrized model.

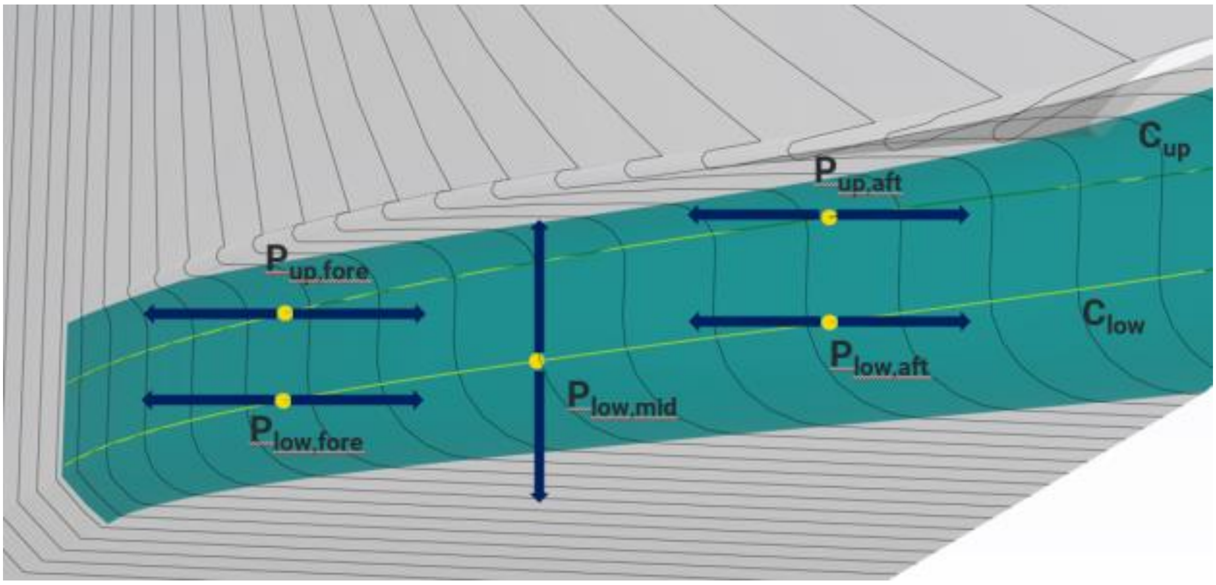

18 | Design variables of the SYN1 partially-parametric model

SYN2: Fully-parametric model

The modelling of the fully-parametric aft ship can be divided into two parts: the bare aft ship, i.e. hull without a skeg, and the skeg geometry itself. While the bare aft ship model was developed from scratch, the skeg was added via a new functionality that was introduced in the Ship Modelling Work-flow of the CAESES 5.3[2] release in January 2025. The following description covers the fundamental ideas behind the model and highlights most important features.

Bare aft ship - geometry curves: The basis for this parametric model is formed by five geometry curves, see figure 19: the deck curve (1), the flat of side (fos) contour (2), the upper (3) and lower (4) tunnel contour and the flat of bottom (fob) contour (5). The lower tunnel contour consists of two curves, an inner and an outer contour, for clarity of the figure only the outer contour is shown.

[2] https://www.caeses.com/downloads/software/software-archive5/CAESES_5.3.4_win64.exe

Funded by the Horizon Europe Programme of the European Union under grant agreement No 101096809
Funded by the Horizon Europe guarantee of the United Kingdom, under project No 10068310
Funded by the Swiss State Secretariat for Education, Research and Innovation

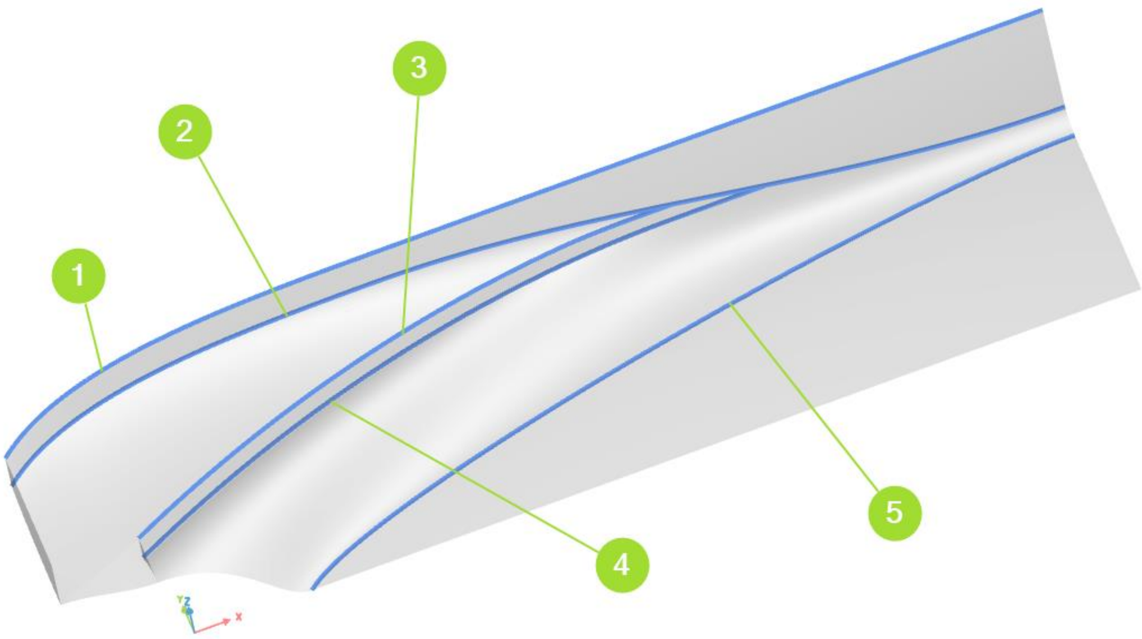

19 | Geometry curves of the bare aft ship of the SYN2 fully-parametric model.

Bare aft ship – surfaces: The geometry curves divide the aft ship in two separate surfaces, a lower surface between fob contour and lower tunnel contour and an upper surface between upper tunnel contour and fos contour, see figure 20 (left).

The lower surface is the most complex surface in this model. It transitions from an S-shape at the transom to the shape of the bilge, see figure 20 (right). The surface is based on sections which are four-point b-splines. The start points of the sections are on the fob curve (5 in figure 19) and the end points on the lower tunnel contour (4 in figure 19). A smooth transition from the reference section at the transom to the bilge is ensured by adjusting the positions of the two mid-points on a curvature continuous path.

The section for the upper surface is a three-point b-spline (figure 20) with the start point on the upper tunnel contour (3 in figure 19) and the end point on the fos contour (2 in figure 19)

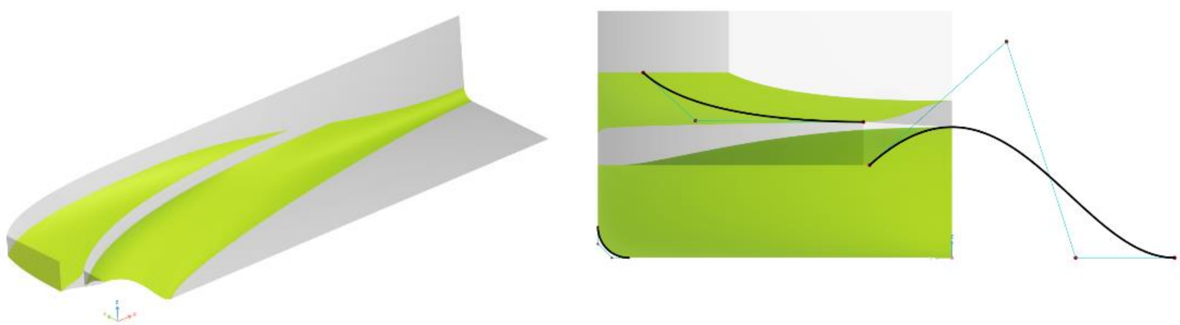

20 | Lower and upper surface of the bare aft ship (left) and sections of the lower and upper surface

Funded by the Horizon Europe Programme of the European Union under grant agreement No 101096809
Funded by the Horizon Europe guarantee of the United Kingdom, under project No 10068310
Funded by the Swiss State Secretariat for Education, Research and Innovation

Skeg - Geometry Curves: The geometry curves for the skeg are displayed in figure 21: reference skeg section (1), propeller hub curve (2), projection curve on the bare aft ship (3), and the combined flat of bottom and centre plane curve (cpc, 4).

Skeg – Surface: The surface of the skeg is created with sections between the projection curve on the bare aft ship (3 in figure 19) and the combined fob and cpc curve (4 in figure 19). With the reference section (1 in figure 19) providing most of the parameters for the shape of the surface.

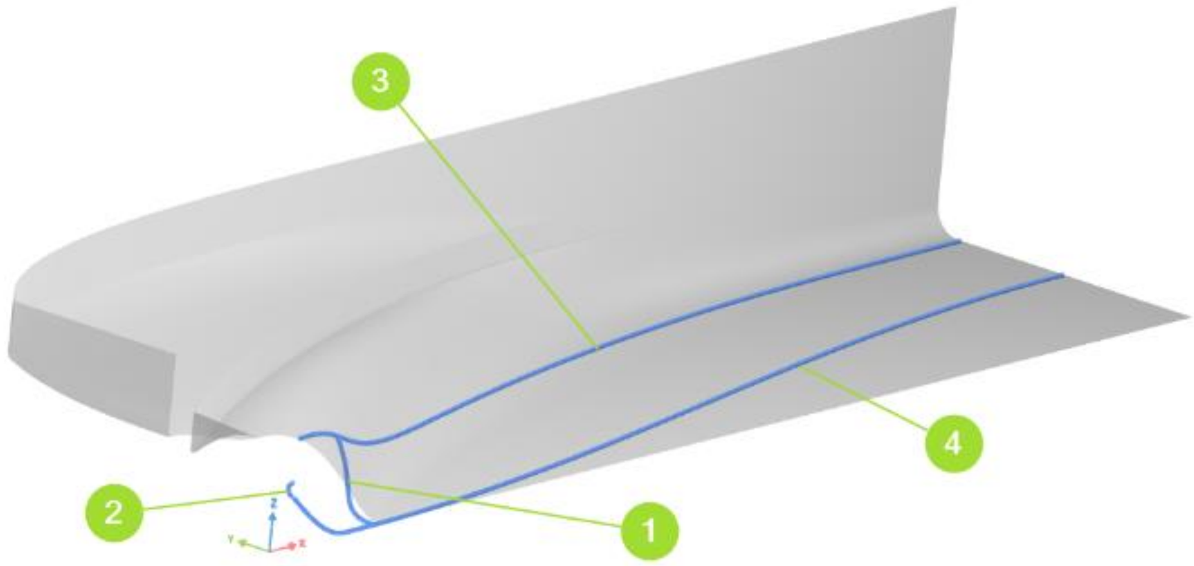

21 | Geometry curve of the skeg

Full Model: To combine both parts, the bare aft ship is trimmed at the projection curve (3 in figure 21). The continuity between the two parts was ensured during the creation of the skeg generation, there the creation of the full aft-ship model simplifies to joining the two parts – bare aft ship and skeg – together, which is shown in figure 22.

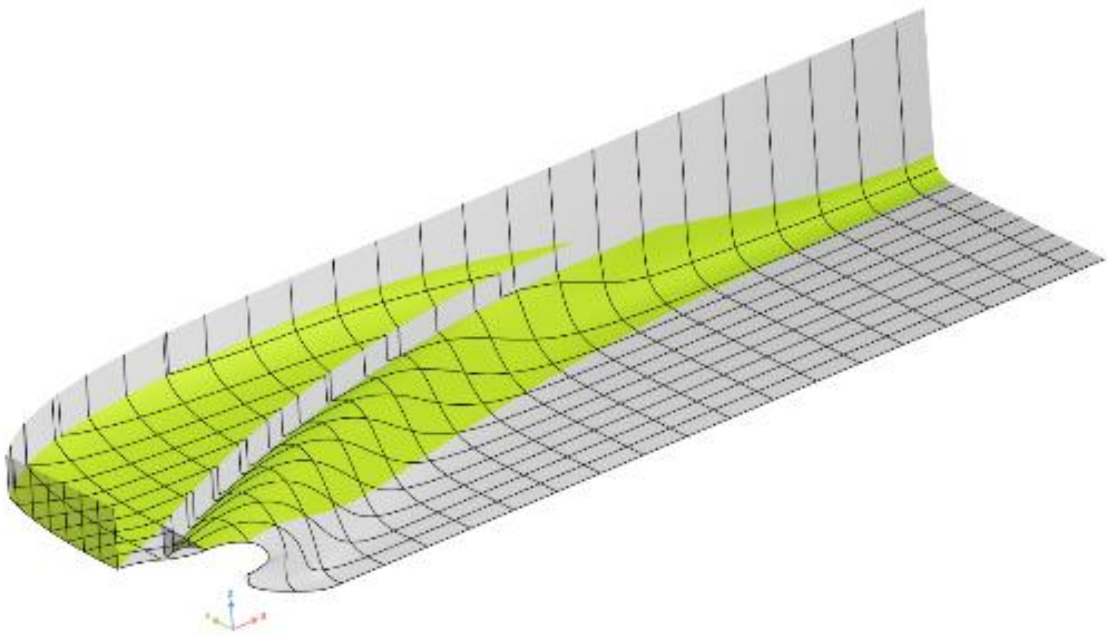

22 | Final aft ship geometry

Funded by the Horizon Europe Programme of the European Union under grant agreement No 101096809
Funded by the Horizon Europe guarantee of the United Kingdom, under project No 10068310
Funded by the Swiss State Secretariat for Education, Research and Innovation

For the optimization study four parameters have been chosen as design variables to control the deformation of the parametrized model. These four parameters control the flat of bottom (curve 5 in figure 19) and tunnel contour (curve 3 and 4 in figure 19) as well as the four-point spline defining the shape of the lower surface (figure 20).

5.6 Optimization Results

5.6.1 SYN1 Variant

The graph in figure 23 shows the results of the optimization process of the parametrized SYN1 variant. Each point represents the result of two simulations, each for design conditions DC1 and DC2 for one individual design, i.e. one unique combination of the five design variables. The values give the percentual change of calculated delivered power ΔPD of that design compared to the SYN1 baseline. On the horizontal axis ΔPD is given for the intermediate water depth, while the vertical axis shows results under the shallow water condition. Thus, lowest left-most points indicate best-performing designs with lowest power demand for both conditions. As both absolute and specific showed very similar trend, for clarity only absolute values (and their relative change) are presented.

In a first step, a design space exploration (DSE) using a Sobol algorithm with quasi-randomly distributed design variables was performed (green points) with a total of 63 investigated valid designs, with a predicted ΔPD ranging between +/-2 percent for DC2 and -4 up to +5% for DC3.

The blue points in figure 23 outline the results generated by the multi-objective global algorithm (MOGA). An accumulation of these blue points can be observed in the lower left area, meaning the RS-generated optimized designs in general outperform the SYN1 baseline, however there can be seen a) a remarkable scatter and b) some outlier with even worse performance compared to the baseline. Investigating the simulations in detail, two reasons were identified: firstly, some noise in the CFD results caused by poorer convergence led to a not so well conditioned RS, which in turn explains the outlier. Especially for the shallow water case (DC3) with its re-markable flow separations the time series calculated with the steady state solver showed relatively large standard deviations. The average of these values was approx. 5 times higher compared to the better performing SYN2 model shown in the subsequent chapter. Secondly a closer look at the correlation of PD on the individual de-sign variables showed the complexity of hull form optimization under shallow water condition.

In the figures 23 and 24 PD is plotted versus the vertical displacement of the lower control curve Clow, for the aft and fore part, resp. The top graphs show values for condition DC2, while for DC3 these are given in the lower graphs. The changing signs of the linear regression trend line (dashed orange curve) in the four graphs impressively show the conflicting correlation of the design variables for the two different water depths: for DC2, the hull lines in the lower aft part should be moved outwards, however for DC3 the lines there should be moved inwards. For the fore part, the dependency is exactly the opposite: DC3 requires slender lines, while it is more beneficial to have blunter lines for DC2 in this area. This clearly demonstrates the strength of such a comprehensive study: knowing both the operational profile and the correlation of the design variables one can use the results of the optimization study to adjust the design to different operational profiles if required.

Funded by the Horizon Europe Programme of the European Union under grant agreement No 101096809
Funded by the Horizon Europe guarantee of the United Kingdom, under project No 10068310
Funded by the Swiss State Secretariat for Education, Research and Innovation

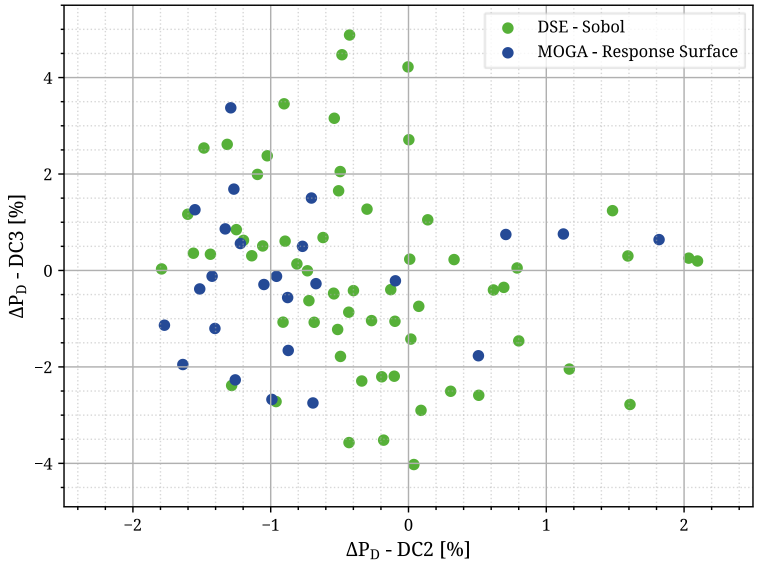

23 | Relative change of PD for DC1 vs DC2 for SYN1.

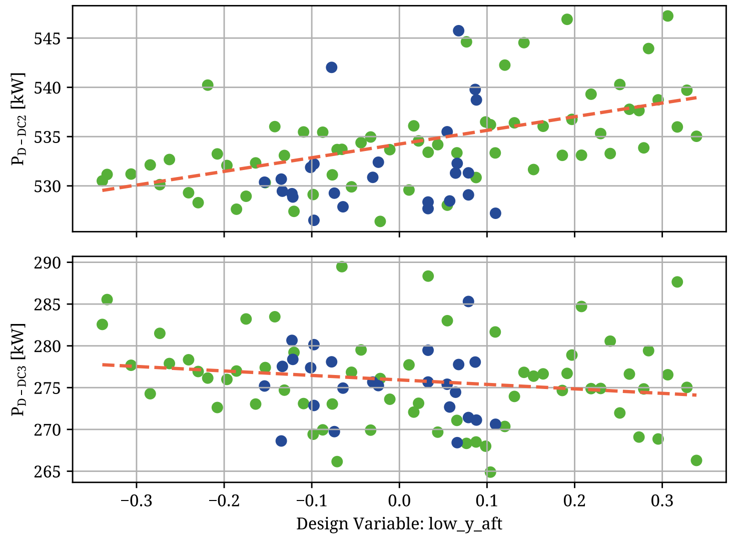

24 | Correlation of PD on the horizontal shift of the lower area for the aft part. Linear regression marked with orange dotted line.

Funded by the Horizon Europe Programme of the European Union under grant agreement No 101096809
Funded by the Horizon Europe guarantee of the United Kingdom, under project No 10068310
Funded by the Swiss State Secretariat for Education, Research and Innovation

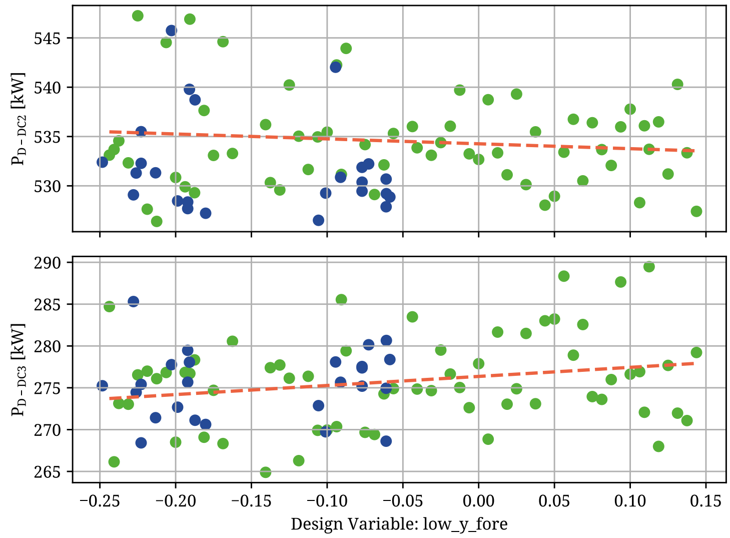

25 | Correlation of PD on the horizontal shift of the lower area for the fore part. Linear regression marked with orange dotted line.

5.6.2 SYN2 Variant

The comparison of the initial variants with the reference vessel in section 5.4 showed a distinct improvement for all three design conditions for the baseline design of SYN2. The additional improvements achieved by optimizing the fully parametrized model with same process (design space exploration in combination with response surface optimization) are given in figure 26. The predicted further reduction of P_D for the best designs lies between 7 to almost 8 % for DC2, and up to 6 % for DC3, compared to the SYN2 baseline. Additionally, there is only marginal scatter of the RS-optimized designs, especially for the intermediate condition DC2, indicating the RS of SYN2 has a more distinct global minimum.

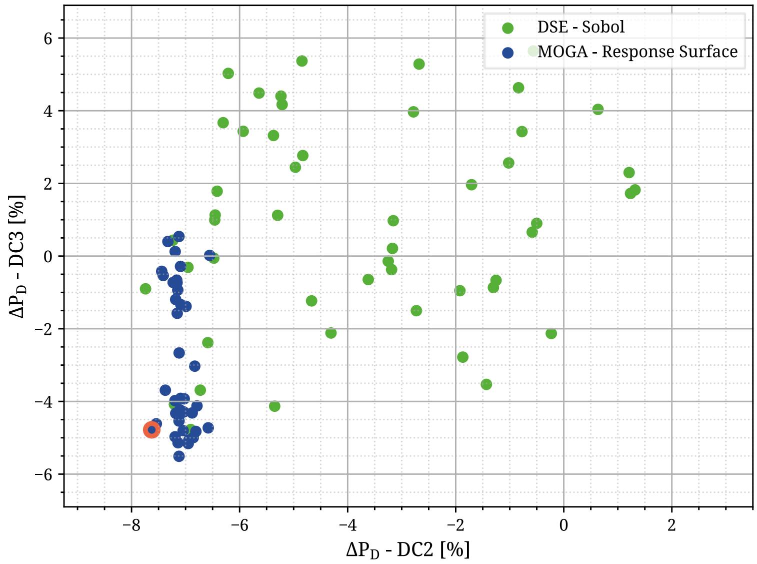

26 | Relative change of PD for DC1 vs DC2 for SYN2

Funded by the Horizon Europe Programme of the European Union under grant agreement No 101096809
Funded by the Horizon Europe guarantee of the United Kingdom, under project No 10068310
Funded by the Swiss State Secretariat for Education, Research and Innovation

5.6.3 Validation

The best design of SYN2 (marked in figure 26 with an orange circle) was selected and further investigated to prove the validity of the simplifications made (predefined, fixed dynamic floating position and double-body), using the same free surface CFD setup as for the baseline comparison. In addition, model tests were done with a newly build physical model, which are described in detail in chapter 6. The values in figure 27 clearly demonstrates that the predicted reductions not only compare well between double body and free surface simulations, but also could be validated with the accompanying model test underlining the success of this optimization study.

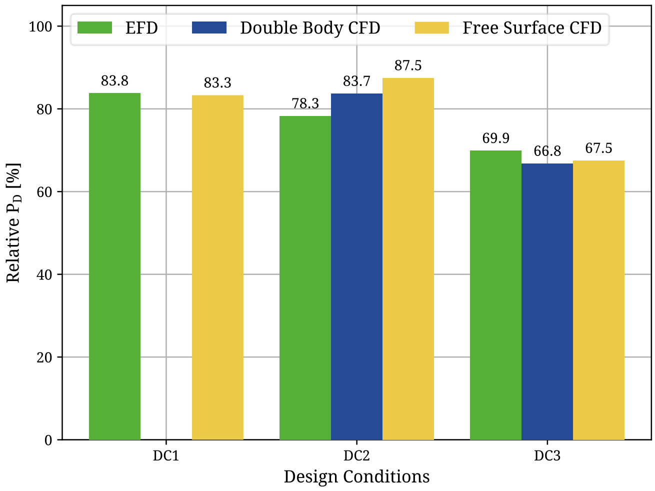

27 | Propulsion Power of the optimized design for the three design conditions in relation to Ernst Kramer (left)

5.6.4 Additional Design Study

Due to the retrofitting both the length of the aft ship and the displacement were fixed as design constraints. Thus, no variation of the aft ship's block coefficient was possible. However, to demonstrate the significant effect of more slender hull lines, the baseline aft ship of SYN1 was stretched by 20 % sacrificing some parallel midship length, which reduces the transport capacity by just 3 tonnes. This modification alone led to a predicted power demand reduction of almost 24 % for the intermediate and around 17.5 % for the shallow water condition, see scatter plot in figure 28. This should be kept in mind to finding best compromise between transport capacity and energy efficiency for design decision of future new buildings.

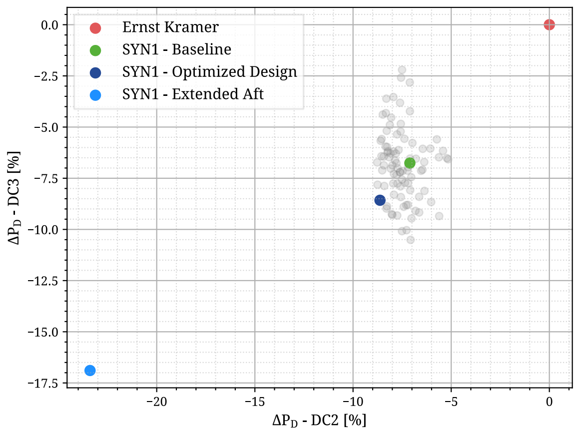

28 | Comparison of calculated propulsion power of extended aft ship.

Funded by the Horizon Europe Programme of the European Union under grant agreement No 101096809
Funded by the Horizon Europe guarantee of the United Kingdom, under project No 10068310
Funded by the Swiss State Secretariat for Education, Research and Innovation

6. Test Campaign with Optimised Aft-Ship

6.1 Experimental Setup and Results

Following the completion of the baseline measurements, the same experimental setup and procedures were applied to test the optimised aft-ship configuration, designated as M2211 (see figure 29). Due to the modular construction of the model, the stern section was replaced directly, while the bow and midship geometry, and testing procedure remained unchanged. All test parameters, including draught, water depth, and vessel speed, were kept identical to those used for the original configuration to ensure direct and reliable comparability.

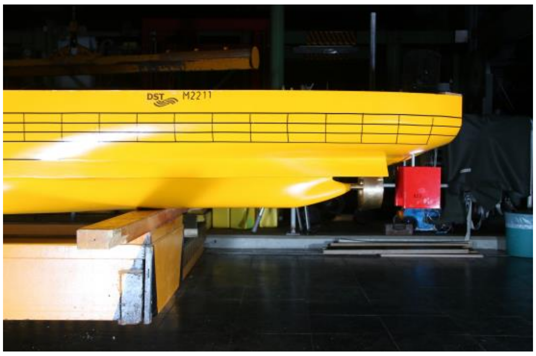

29 | Optimized aft-ship model configuration (M2211) during preparation for testing at DST.

The objective of the optimization was to reduce delivered power requirements under typical operational conditions by improving the flow characteristics at the stern, particularly under shallow and transitional depth conditions. The resulting performance of the optimised configuration (M2211) is presented in figure 30.

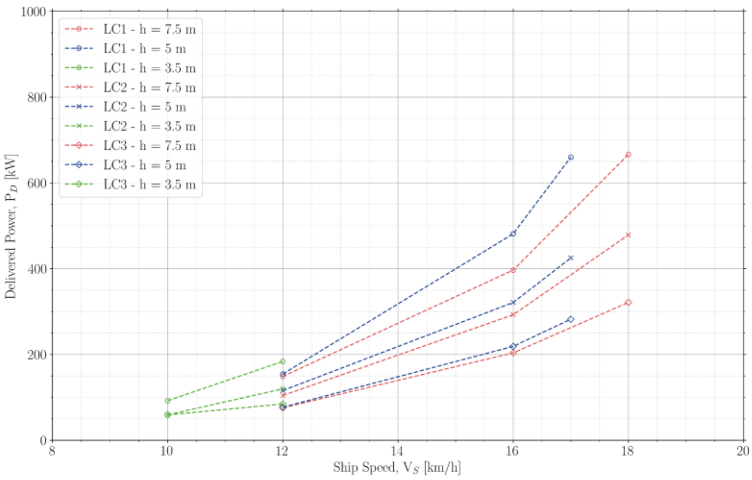

30 | Predicted power demand in the full scale for the optimized aft-ship model (M2211) across various loading conditions, water depths, and vessel speeds.

Funded by the Horizon Europe Programme of the European Union under grant agreement No 101096809
Funded by the Horizon Europe guarantee of the United Kingdom, under project No 10068310
Funded by the Swiss State Secretariat for Education, Research and Innovation

In LC1 - representing full load (T = 2.8 m) - the influence of shallow water remains clearly present. At 12 km/h, delivered power increases from 148.9 kW in deep water (h = 7.5 m) to 183.7 kW in shallow water (h = 3.5 m), a rise of nearly 23.4%. At lower speeds, the difference is also noticeable: at 10 km/h in h = 3.5 m, power demand is 92.3 kW, while no test was conducted in deeper water due to lower expected resistance. At higher speeds, the differences are even more pronounced: for example, at 16 km/h, the required power rises from 396.7 kW (h = 7.5 m) to 481.3 kW (h = 5 m), corresponding to a 21.3 % increase.

LC2, corresponding to partial loading (T = 1.9 m), follows the same trend with lower absolute values. At 12 km/h, delivered power increases from 104.4 kW (h = 7.5 m) to 115.9 kW (h = 5 m) and 119.9 kW (h = 3.5 m), representing a total increase of approximately 14.9 % from deep to shallow water. At 16 km/h, the power demand increases from 292.6 kW to 321.2 kW, which equals a 9.8% rise.

In LC3, simulating an empty vessel with trim by stern (T_A = 1.35 m, T_F = 0.75 m), the lowest delivered power values were recorded. At 12 km/h, power increased from 75.5 kW (h = 7.5 m) to 84.5 kW (h = 3.5 m) - a rise of 11.9 %.

6.2 Comparative Results and Performance Gains

The comparative evaluation of the original (M2202) and optimised (M2211) aft-ship configurations was performed across three representative loading conditions, varying water depths, and a range of vessel speeds. The results consistently demonstrate the benefits of the optimised stern geometry, particularly under shallow water conditions and higher loading scenarios.

LC1 - representing full load (T = 2.8 m) - the most significant improvements were recorded (see Figure 30). At 12 km/h in shallow water (h = 3.5 m), the delivered power was reduced by over 30 %, while in deep water the reduction exceeded 15 %. Even at lower speeds, such as 10 km/h, the optimised configuration showed a reduction in power demand of nearly 27 %. These findings confirm the strong influence of hull form on hydrodynamic resistance in high-draught, restricted-depth conditions.

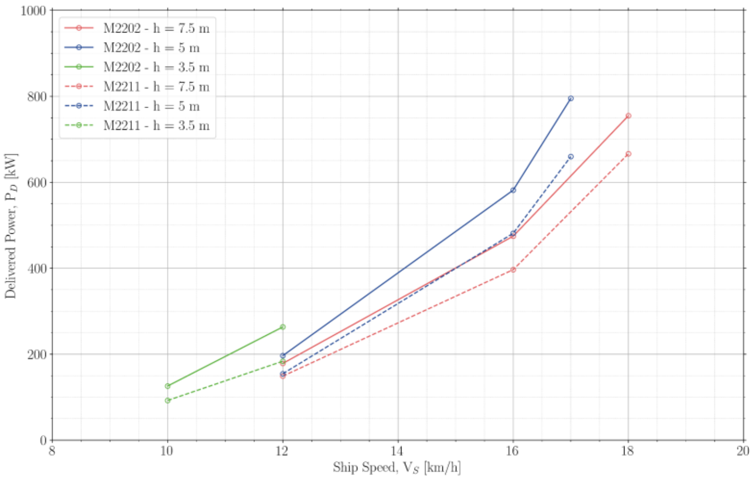

31 | Comparison of delivered propulsion power for M2202 and M2211 in LC1 (full load) across different water depths and speeds.

In LC2 - corresponding to partial load (T = 1.9 m) - the improvements were moderate but consistent (see Figure 32). Power savings typically ranged between 10 % and 20 %, depending on the depth and speed. In more constrained depths (h = 3.5 m), the improvement reached 31.6 % at 10 km/h, demonstrating that optimisation is still effective under lightened loading when combined with shallow water.

Funded by the Horizon Europe Programme of the European Union under grant agreement No 101096809
Funded by the Horizon Europe guarantee of the United Kingdom, under project No 10068310
Funded by the Swiss State Secretariat for Education, Research and Innovation

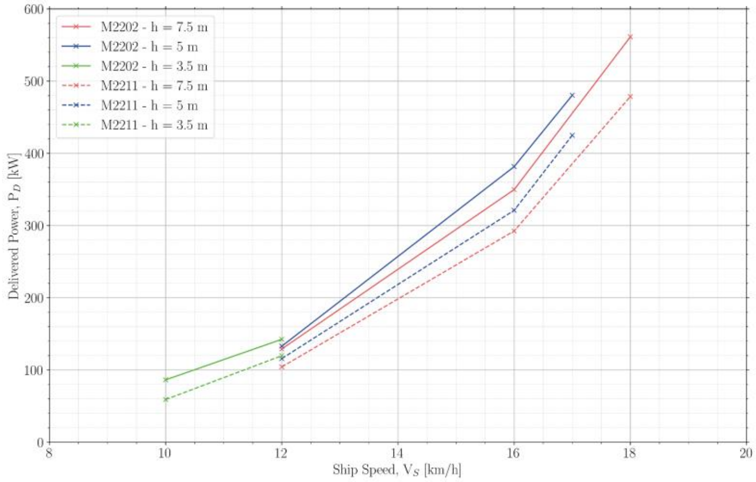

32 | Comparison of delivered propulsion power for M2202 and M2211 in LC2 (partial load) across different water depths and speeds.

In LC3 - representing the light ship condition with trim by stern - although the absolute power levels were the lowest, relative savings remained relevant (see Figure 33). Reductions of up to 21% were observed at higher speeds, while at moderate speeds (12 km/h), improvements ranged between 12% and 16%, depending on water depth.

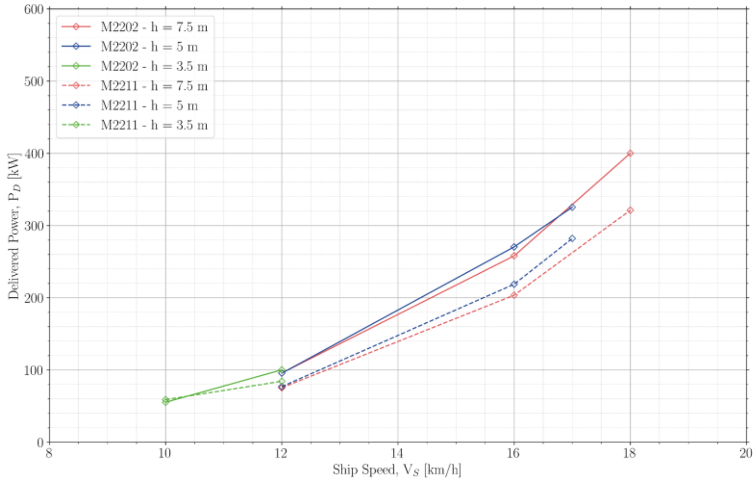

33 | Comparison of delivered propulsion power for M2202 and M2211 in LC3 (light ship with trim by stern) across different water depths and speeds.

Only one outlier was observed: at 10 km/h in h = 3.5 m, a slight increase in delivered power was recorded for the optimised configuration. This deviation is not indicative of a performance shortfall but rather a ventilation phenomenon. In this specific case, air was entrained at the stern, disrupting the propeller inflow and increasing resistance. The modified geometry, although more efficient in general, did not allow air bubbles to detach and dissipate effectively, resulting in a temporary rise in propulsion power. Supporting visualisation provided in figure 34, which highlight the flow disturbance and air pocket formation observed during the tests.

Funded by the Horizon Europe Programme of the European Union under grant agreement No 101096809
Funded by the Horizon Europe guarantee of the United Kingdom, under project No 10068310
Funded by the Swiss State Secretariat for Education, Research and Innovation

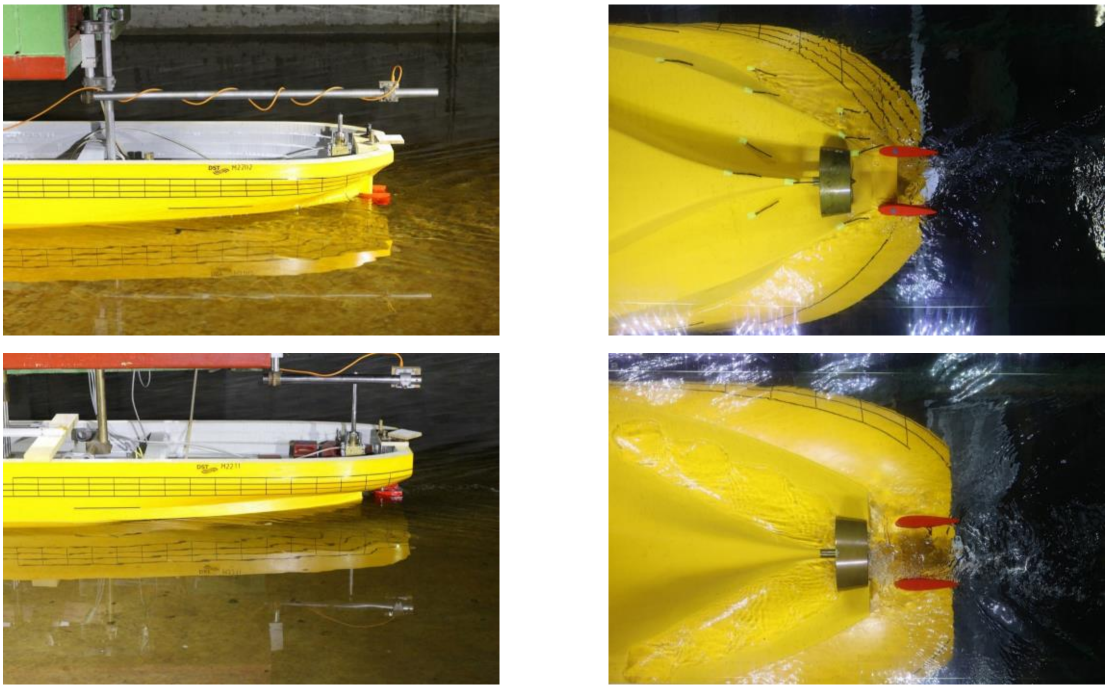

34 | Loading Condition 3 (LC3), h=3.5 m at 10 km/h. Original configuration M2202 (top) - clean stern flow and no visible ventilation. Optimised configuration M2211 (bottom) - air entrainment and disturbed wake.

Across all tested scenarios, the optimised configuration (M2211) demonstrated consistent and meaningful improvements in propulsion efficiency. A detailed overview of relative performance gains for each tested condition is provided in table 8. The most pronounced gains were observed under full load in shallow water (as illustrated in Figure 35), reflecting the most hydrodynamically challenging conditions. These results confirm the effectiveness of the optimisation strategy and its relevance for inland waterway vessels, where hull–propeller interaction and restricted under-keel clearance play a dominant role.

35 | Loading Condition 1 (LC1), h=3.5m at 12km/h. Experimental verification of the optimisation results in DST’s large shallow water basin. The smooth ship wake for the new design (M2211) on the right can be noticed.

Overall, reductions in delivered power typically ranged between 15% and 30%, depending on the specific combination of draught, water depth, and vessel speed. These improvements translate directly into lower energy demand and fuel consumption, offering tangible environmental and economic benefits.

Funded by the Horizon Europe Programme of the European Union under grant agreement No 101096809
Funded by the Horizon Europe guarantee of the United Kingdom, under project No 10068310
Funded by the Swiss State Secretariat for Education, Research and Innovation

8 | Relative difference in delivered propulsion power [%] between the original (M2202) and optimised (M2211) aft-ship configurations across various loading conditions, water depths (h), and vessel speeds (V). Positive values indicate power savings achieved with the optimised design. Empty cells indicate that model tests were not conducted for the corresponding combination of parameters.

Loading Condition	h [m]	V [km/h]				
		10	12	16	17	18
LC1	3.5	26.69	30.26			
	5		21.41	17.26	17.01	
	7.5		16.58	16.41		11.74
LC2	3.5	31.56	15.92			
	5		12.92	15.85	11.53	
	7.5		19.26	16.38		14.73
LC3	3.5	-6.49	15.75			
	5		19.44	19.11	13.3	
	7.5		21.27	21.11		19.72

Funded by the Horizon Europe Programme of the European Union under grant agreement No 101096809
Funded by the Horizon Europe guarantee of the United Kingdom, under project No 10068310
Funded by the Swiss State Secretariat for Education, Research and Innovation

7. New engine layout and business case

Following the hydrodynamic optimisation of the aft-ship, a new engine configuration was proposed to further enhance the vessel's operational efficiency. The original setup, based on a single 1170 kW main engine, was replaced by a twin-engine arrangement commonly referred to as "Father & Son". This consists of a 735 kW primary engine and a 368 kW auxiliary engine, allowing flexible power deployment depending on the operational demand.

7.1 Current installation

The current propulsion system of the Ernst Kramer relies on a single Mitsubishi Heavy Industries S16R-MPTA main engine rated at 1170 kW at 1600 rpm. While this high-power configuration ensures sufficient performance reserves, onboard operational data indicate that the engine operates far below its rated capacity for most of the time. This mismatch results in suboptimal fuel efficiency and elevated specific emissions during typical inland navigation cycles.

To align installed power with actual operational demand, alternative engine configurations were considered. Specifically, three Stage V-certified engines from the MAN portfolio were selected for further evaluation: D2676LE457 (221 kW), D2676LE47A (368 kW), and D2862LE44A (735 kW). Their technical specifications are summarised in table 9. Notably, detailed fuel consumption curves and load-dependent performance characteristics for these engines are publicly available via the official MAN Engines website.

9 | Specifications of selected MAN engines [10].

Performance data	Unit	D2676LE457 221Kw	D2676LE47A 368kW	D2862LE44A 735kW
Rated power	kW	221	368	735
Rated power	PS	301	500	1000
Speed	rpm	1800	1800	1800
Bore/Stroke	mm	126/166	126/166	128/157
Displacement	litre	12.42	12.42	24.24
Rated torque	Nm	1172	1952	3900
Maximum torque	Nm	1320	2200	4388
at speed	rpm	1000-1600	1400-1600	1300-1600
Compression ratio	:1	18	18	19
Mean effective pressure	bar	12	20	20
Mean piston speed	m/s	10	10	9
Specific fuel consumption	g/kWh	207	200	196
Absolute fuel consumption	l/h	54	88	172
Lowest fuel consumption	g/kWh	206	198	195
Absolute urea consumption	l/h	4	7	10

To evaluate the suitability of each engine in a standalone arrangement, their performance was assessed against the actual power demand profile recorded onboard for one year. The annual distribution of engine load was calculated individually for the 221 kW, 368 kW, and 735 kW engines, assuming they operate alone. Results, shown in figure 36, indicate that none of the selected engines alone can efficiently cover the full operational range:

Funded by the Horizon Europe Programme of the European Union under grant agreement No 101096809
Funded by the Horizon Europe guarantee of the United Kingdom, under project No 10068310
Funded by the Swiss State Secretariat for Education, Research and Innovation

- 221 kW: Overloaded for more than 60 % of the time, clearly undersized.
- 368 kW: Also overloaded in approximately of 46 % of operational time.
- 735 kW: More suitable for high-power scenarios; inefficient at low loads.

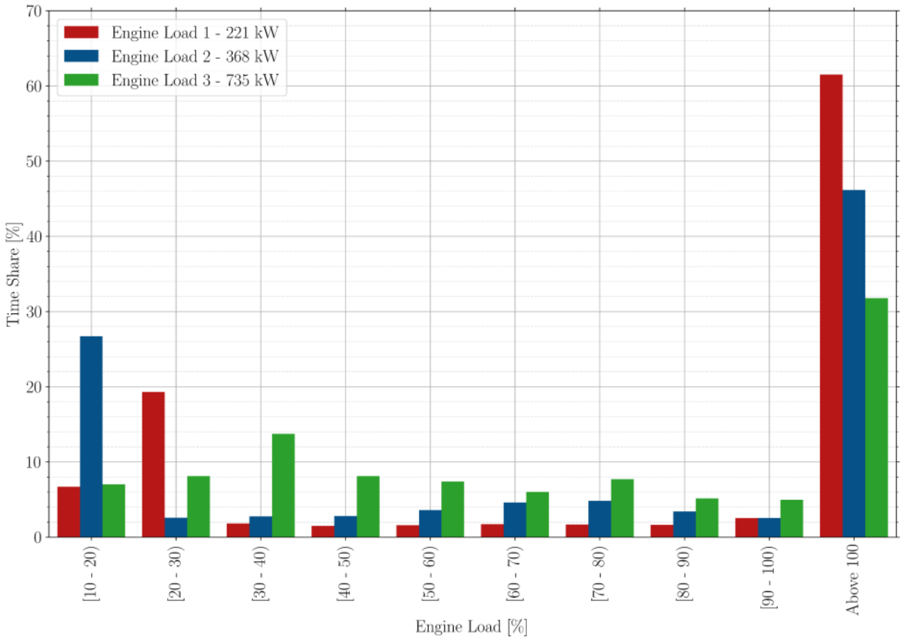

36 | Distribution of engine load [%] over one year of operation for three standalone engine configurations (221 kW, 368 kW, and 735 kW). Each bar represents the percentage of operational time spent within a specific load interval. Results refer to the original hull.

These findings confirm that a standalone configuration leads to inefficiencies. Consequently, a dual-engine "Father & Son" layout was selected, comprising a 735 kW "Father" and a 368 kW "Son" engine. The operational logic of the Father-Son concept is structured around three load cases:

1. **Case 1** - Low Power Demand (≤ 90% of Son capacity): Only the 368 kW engine is active, operating efficiently in low-load canal navigation.
2. **Case 2** - Medium Power Demand (331–661 kW): The 735 kW engine operates alone, maintaining optimal efficiency without engaging the smaller engine.
3. **Case 3** - High Power Demand (≥ 90% of Father capacity): Both engines are activated. The larger engine is fixed at 90% load, and the smaller engine delivers the remaining required power.

The resulting load distribution (figure 37) confirms the effectiveness of this approach:

- The 368 kW engine primarily operates in the [10–20] % and [20–80] % ranges (37 % and 43 % of the time, respectively), covering low to moderate power demand efficiently.
- The 735 kW engine predominantly operates in the [80–90] % range (58 %), optimally supporting high-demand segments such as upstream Rhine navigation.

Funded by the Horizon Europe Programme of the European Union under grant agreement No 101096809
Funded by the Horizon Europe guarantee of the United Kingdom, under project No 10068310
Funded by the Swiss State Secretariat for Education, Research and Innovation

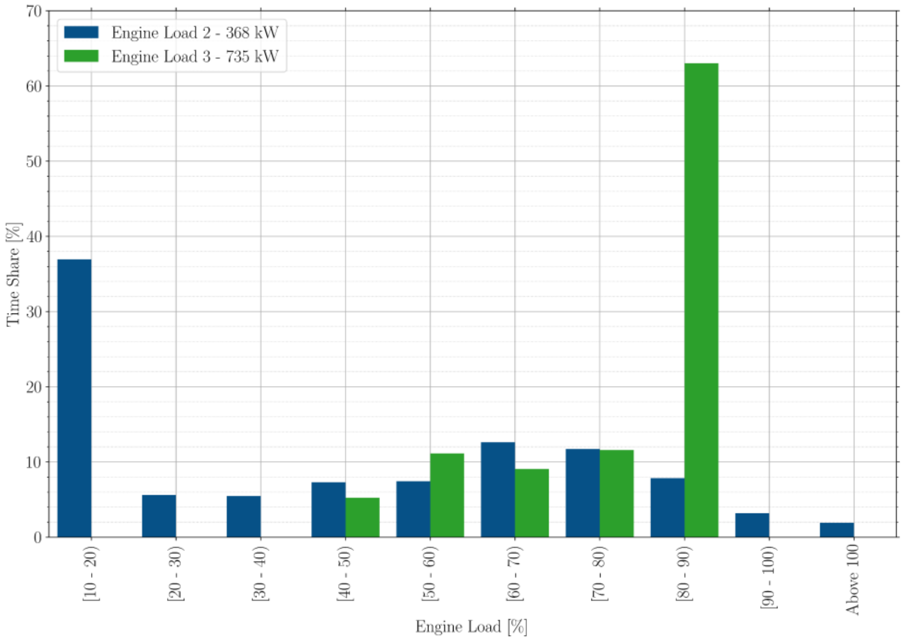

37 | Distribution of engine load [%] over one year of operation for the Father & Son propulsion configuration (368 kW + 735 kW). Each bar represents the percentage of operational time spent within a specific load interval. Results refer to the original hull.It should be noted that the presented load distributions are derived from operational data corresponding to the vessel's original hull form. Following hull optimization, a reduction in overall power demand is expected, which will further enhance the efficiency and load balance of the selected propulsion system.

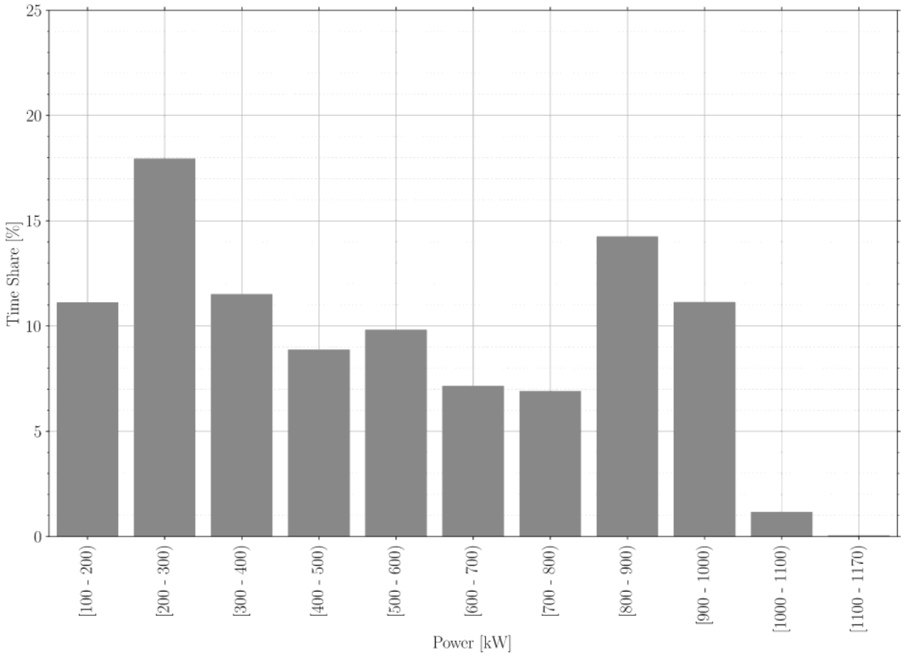

38 | Distribution of propulsion power demand throughout the full dataset.

Funded by the Horizon Europe Programme of the European Union under grant agreement No 101096809
Funded by the Horizon Europe guarantee of the United Kingdom, under project No 10068310
Funded by the Swiss State Secretariat for Education, Research and Innovation

As shown in figure 38, propulsion activity is predominantly concentrated in the [200–400) kW range, which accounts for approximately 41% of operational time and aligns with the efficient operating envelope of the 368 kW (Son) engine. A secondary peak appears in the [400–800) kW range (~33 %), reflecting higher power demand typically associated with upstream navigation or acceleration, where the 735 kW (Father) engine is more suited. Power demands beyond this range are covered by the combined operation mode.

7.2 Evaluation Based on Operational Profiles

To assess the performance of the modular propulsion system under realistic operational conditions, three representative voyages were selected based on actual onboard measurements. These included canal transit, upstream navigation, and downstream navigation, thereby covering the full spectrum of typical inland waterway transport scenarios.

The analysis combines full-scale operational data with scaled model test results and analytical fuel consumption modelling. As model tests were conducted in calm water without external influences like current, the delivered power values were uniformly increased by 15 % to better reflect the resistance experienced under real-world conditions. This correction was applied consistently to both the original and optimized hull configurations. Due to the lack of water current measurements in the onboard dataset, the actual speed through water could not be determined directly, so that the vessel speed had to be estimated indirectly. For each time step in the operational dataset, the measured delivered propulsion power was matched to the closest available draught-depth combination from the scaled original hull test matrix. Using cubic polynomial interpolation fitted to the model test data, the vessel speed corresponding to the measured delivered power was numerically estimated via root-finding. This estimated speed was then used to determine the corresponding delivered power on the optimized hull form by evaluating the equivalent polynomial from the scaled optimized test data.

This approach enabled consistent estimation of the hypothetical power requirement with the optimized aft-ship, assuming identical vessel speed and loading. The resulting optimized power values were then used as input for an analytical fuel consumption model, which simulated engine load, and fuel consumption for each engine configuration (Father, Son, or combined mode).

1. Canal Voyage (Berlin – Duisburg)

This voyage in the Mittelland Canal, Germany, represents typical low-speed, steady-state navigation through confined and shallow waterways. The vessel travelled over five days, with an average speed of 9.7 km/h. The vessel's average draught during the voyage was 2.45 m.

Funded by the Horizon Europe Programme of the European Union under grant agreement No 101096809
Funded by the Horizon Europe guarantee of the United Kingdom, under project No 10068310
Funded by the Swiss State Secretariat for Education, Research and Innovation

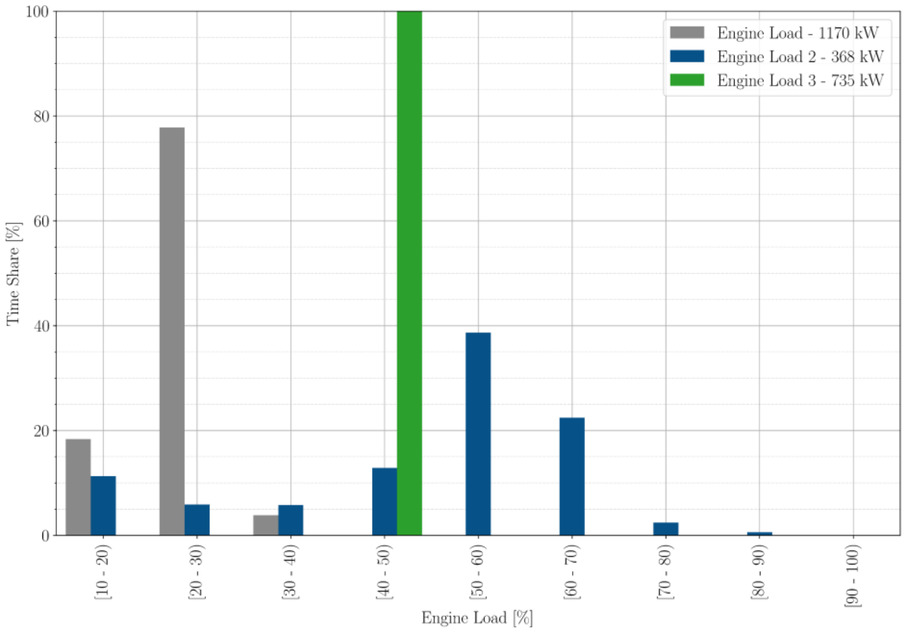

39 | Distribution of engine load [%] during the canal voyage for three propulsion setups : original engine (1170 kW), Son engine (368 kW), and Father engine (735 kW). Each bar represents the share of time spent in a given load band only when the engines would be active.

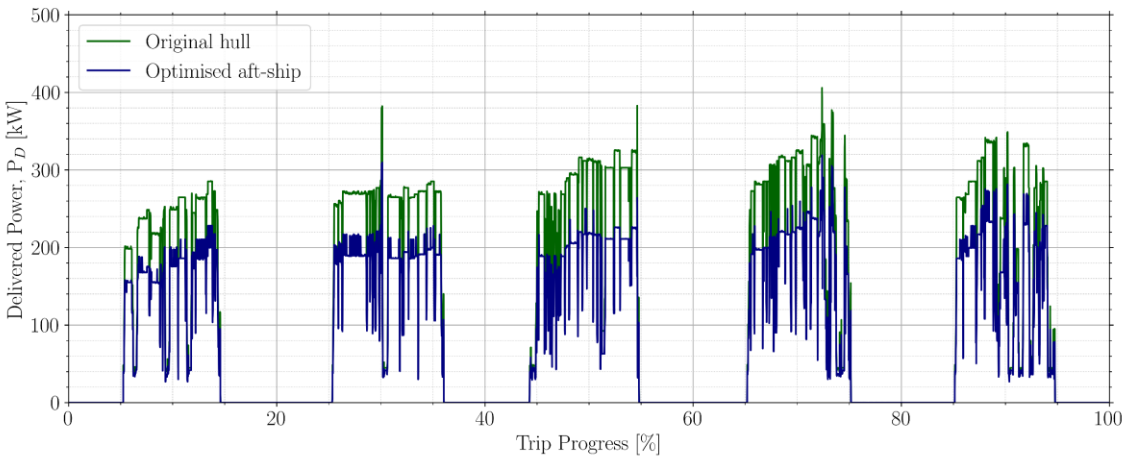

40 | Delivered power over trip progress [%] for the canal voyage , comparing the original hull (green) and optimised aft-ship (blue).

Under these conditions, the original 1170 kW main engine operated far below its optimal efficiency range. As shown in figure 37, 78 % of propulsion time occurred in the [20–30) % load band, with an additional 18 % below 20 %. Such low load levels result in poor combustion efficiency, elevated specific fuel consumption, and increased emissions. By contrast, the modular Father & Son arrangement significantly improved the load distribution. The smaller 368 kW engine (Son) handled the propulsion alone for most of the time, operating between 20 % and 70 % load for over 95 % of the voyage. The larger 735 kW engine (Father) was engaged only briefly, operating exclusively in the [40–50) % load band, and remained idle for the rest of the trip. The comparative delivered power profile between the original and optimised aft-ship is shown in figure 39. The optimised hull consistently required lower delivered power.

Funded by the Horizon Europe Programme of the European Union under grant agreement No 101096809
Funded by the Horizon Europe guarantee of the United Kingdom, under project No 10068310
Funded by the Swiss State Secretariat for Education, Research and Innovation

These results confirm that the original engine is oversized for canal navigation. The modular propulsion layout allows for precise power matching, ensuring that engines operate within their most efficient range. The outcome is reduced fuel consumption, lower emissions, and decreased engine wear. This is particularly relevant for frequent low-speed operations in inland waterways.

2. Upstream Voyage (Rotterdam - Mannheim)

The voyage represents a high-load operational scenario, with the vessel sailing continuously upstream along the Rhine River. The journey covered approximately 580 km in 5 days, with an average speed of 10.2 km/h and an average draught of 2.61 m, indicating near full-load conditions. The delivered propulsion power required by both the original and optimised hull configurations throughout the voyage is presented in figure 42.

Under these demanding conditions, see figure 41, the original 1170 kW engine operated predominantly in the high-load range, spending over 78 % of the time above 70 % MCR and nearly 50 % in the [80–90) % interval. Although this regime is within the efficient range for these engines, such sustained loading implies prolonged mechanical stress. In contrast, the Father & Son configuration achieved a more balanced power distribution between the two engines. The 735 kW engine (Father) carried the primary load, operating mainly between 70 % and 90 % of its rated capacity, which is optimal for this type of voyage. The smaller 368 kW engine (Son) was primarily active during transitional phases, such as lock approaches and velocity modulation, contributing in the [20–50) % load range for approximately 59 % of its active time. Instances of suboptimal operation below 20 % load were observed but were limited to brief durations.

The dual-engine layout successfully reduced continuous peak loading on a single engine and avoided typical low-load inefficiencies associated with oversized configurations. However, further refinement of the engine activation logic may be warranted to reduce unnecessary low-load operation of the Son engine, particularly since the Father engine can sustain operation at full capacity when required. Such adjustment could further improve overall fuel efficiency.

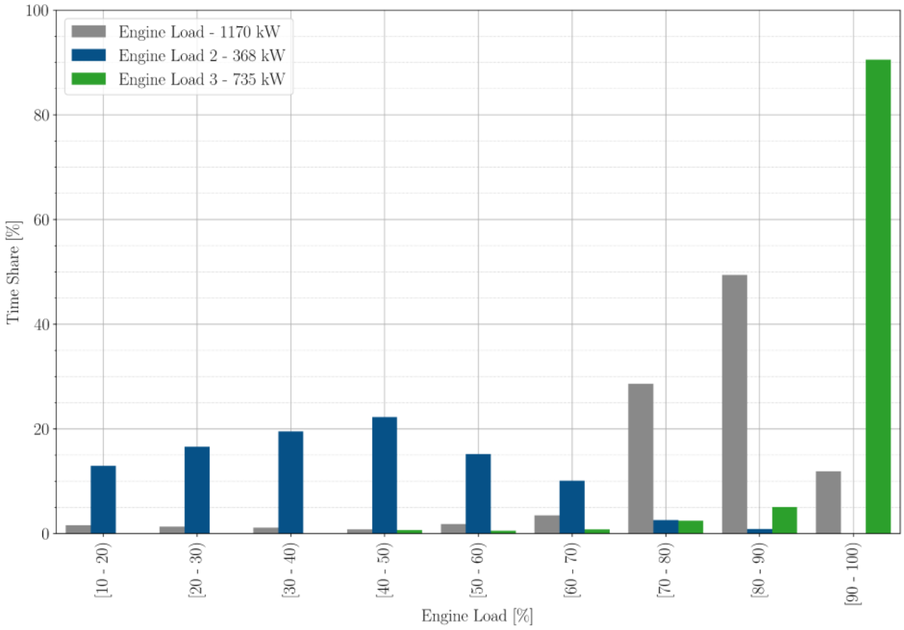

41 | Distribution of engine load [%] during the upstream voyage for three propulsion setups: original engine (1170 kW), Son engine (368 kW), and Father engine (735 kW). Each bar represents the share

Funded by the Horizon Europe Programme of the European Union under grant agreement No 101096809
Funded by the Horizon Europe guarantee of the United Kingdom, under project No 10068310
Funded by the Swiss State Secretariat for Education, Research and Innovation

of time spent in a given load band only when engines would be active.

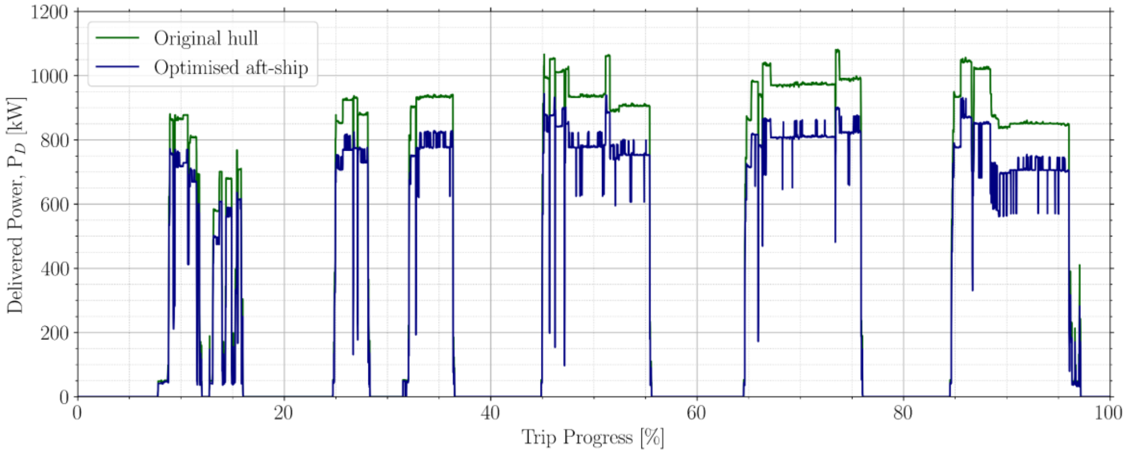

42 | Delivered power over trip progress [%] for the upstream voyage , comparing the original hull (green) and optimised aft-ship (blue).

3. Downstream Voyage (Mannheim - Rotterdam)

The downstream voyage followed the same Rhine route in reverse, from Mannheim to Rotterdam. The scenario represents medium to high-speed operation under reduced resistance conditions. The vessel sailed 594 km over 33.7 hours, with an average speed of 17.6 km/h and an average draught of 2.40 m, indicating a moderate loading condition. Compared to the upstream journey, this downstream passage was completed approximately one day faster. This can be seen in the delivered power time series (figure 44), where one operational segment is visibly absent. It can be observed as well that optimised hull consistently required lower delivered power.

The original 1170 kW engine operated mainly in the [60–70) % load range (49.7 % of the time), which aligns with its efficient zone (figure 43). However, around 20 % of its operation occurred below 40 % load, indicating periods of low propulsion resistance where the engine likely consumed fuel inefficiently.

Funded by the Horizon Europe Programme of the European Union under grant agreement No 101096809
Funded by the Horizon Europe guarantee of the United Kingdom, under project No 10068310
Funded by the Swiss State Secretariat for Education, Research and Innovation

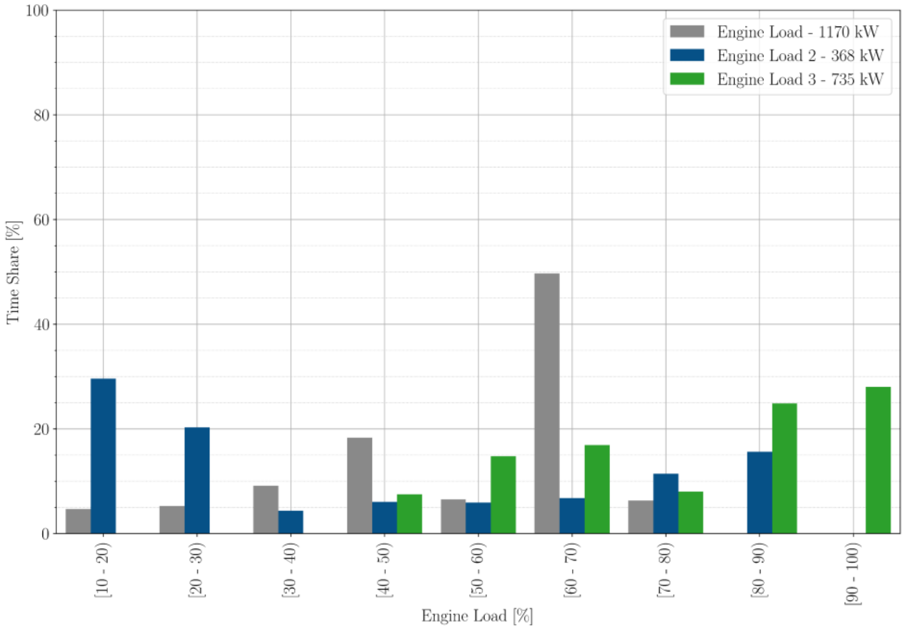

43 | Distribution of engine load [%] during the downstream voyage for three propulsion setups: original engine (1170 kW), Son engine (368 kW), and Father engine (735 kW). Each bar represents the share of time spent in a given load band only when the engines would be active.

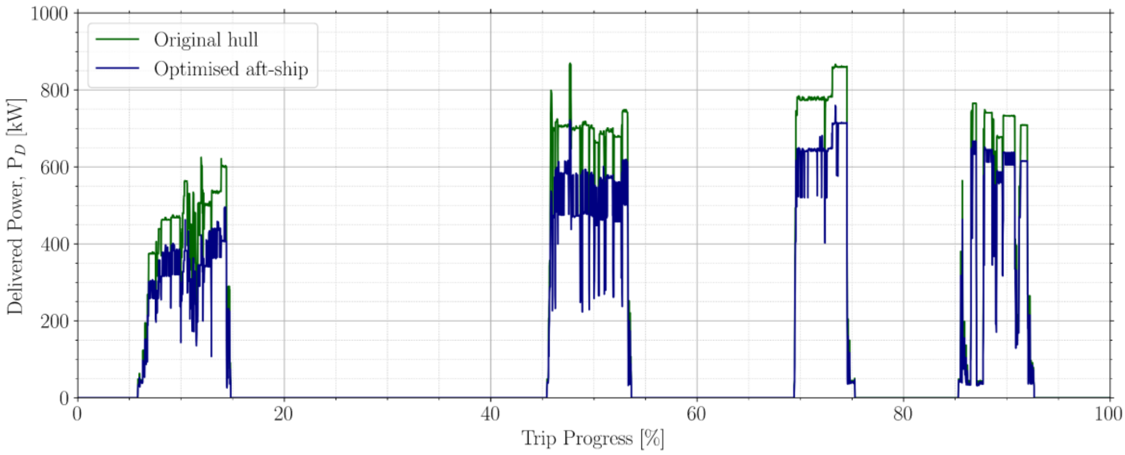

44 | Delivered power over trip progress [%] for the downstream voyage , comparing the original hull (green) and optimised aft-ship (blue).

In contrast, the modular Father & Son propulsion system exhibited a divided load profile. The larger 735 kW engine (Father) operated predominantly in the [80–100) % range, maintaining efficient performance during high-demand segments. The smaller 368 kW engine (Son), however, lacked a dominant operational band, spending nearly 30 % of its active time in the [10–20) % range and showing fragmented usage across other bands. While the Father engine remained within its optimal regime, the Son engine's deployment appeared suboptimal.

The available data suggests that propulsion demand may have been allocated to the larger engine even in conditions where the Son engine could have operated more efficiently. This reduces the efficiency advantages of the modular system and highlights the need to improve how power is shared between engines, especially during downstream trips with fast-changing power demand due to river current.

Funded by the Horizon Europe Programme of the European Union under grant agreement No 101096809
Funded by the Horizon Europe guarantee of the United Kingdom, under project No 10068310
Funded by the Swiss State Secretariat for Education, Research and Innovation

7.3 Engine Usage and Fuel Consumption Assessment

To complement the analysis presented in the previous sections, engine usage patterns and fuel consumption were examined across the three representative voyages; canal, upstream, and downstream. This dual assessment enables a holistic evaluation of both operational behaviour and energy efficiency gains achieved through the modular propulsion system and hull optimisation.

The engine usage was categorised into four modes: only the Son engine (368 kW) active, only the Father engine (735 kW) active, both engines active, and idle. The relative time spent in each mode is summarised in table 10.

10 | Engine operation time share [%] for each voyage type. Results refer to the optimized hull.

Voyage Type	Son Active	Father Active	Both Active	Idle
Canal	50.2	0.01	0.00	49.8
Upstream	5.8	4.3	40.8	49.1
Downstream	9.0	15.4	6.0	69.6

The dual-engine system demonstrates a high degree of operational flexibility. In canal navigation, the low power demand is efficiently met by the Son engine alone, resulting in a favourable engine load profile and minimised fuel consumption. During upstream navigation, the system responds correctly by activating both engines for prolonged periods to meet the high and continuous power demand. Although this leads to higher absolute fuel consumption, it is justified from an operational standpoint and indicates that the system is correctly dimensioned for such scenarios.

In downstream navigation, the system primarily relied on the larger Father engine, while the Son engine was rarely used. Although this may appear inefficient, operating a single engine near its optimal load point is often more economical than splitting the load across two engines or running engines with higher installed power at low load.

To quantify the benefits of both the optimised aft-ship and modular propulsion system, fuel consumption was compared under four scenarios:

1. **Baseline**: Actual onboard fuel consumption with the original 1170 kW engine.
2. **Aft-ship only**: Simulated consumption with optimised hull, original engine retained.
3. **Father–Son only**: Simulated consumption using modular engine layout, original hull retained.
4. **Combined**: Simulated with both hull and engine configuration optimised.

11 | Comparison of baseline layout to optimised options

Voyage	Baseline [L]	Aft Only [L]	F–S Only [L]	Combined [L]
Canal	3864	2911 (↓24.7%)	3291 (↓14.8%)	2590 (↓33.0%)
Downstream	5183	4125 (↓20.4%)	4940 (↓4.7%)	3969 (↓23.4%)
Upstream	13043	10943 (↓16.1%)	12538 (↓3.9%)	11403 (↓12.6%)

Funded by the Horizon Europe Programme of the European Union under grant agreement No 101096809
Funded by the Horizon Europe guarantee of the United Kingdom, under project No 10068310
Funded by the Swiss State Secretariat for Education, Research and Innovation

The highest relative fuel saving was recorded during canal navigation. This is attributed to the operation of the Son engine within its most efficient range, enabled by low propulsive power demand. In downstream navigation, although resistance was reduced due to flow conditions, the observed inefficiencies in engine allocation limited the achievable savings. For the upstream voyage, where high continuous power was required, both engines operated jointly for long durations. In this case, most savings resulted from the reduced hull resistance achieved through aft-ship optimisation.

7.4 Business Case.

When all the savings achieved through changes to the stern geometry, new propulsion systems and the proportionate use of HVO are added together, it becomes clear that even with more 'conventional' measures, a 35 % reduction in harmful emissions and climate-impacting emissions can be achieved. There is therefore also a relatively inexpensive way to achieve the goals of the Mannheim Declaration [11] for 2035. This section will now show the approximate costs to be expected and the extent to which the measures are economically viable.

The conversion of the stern to the new geometry is expected to cost around one million euros. Since the position of the propeller will not be changed, it would be possible to simply remove the plates, renew the frame contour and then attach new plates. The price of steel, including processing, would be around EUR 20 per kg for this option. By comparison, a completely new stern with a new cabin and new wheelhouse would cost between 4 million EUR and 4.5 million EUR. However, everything would then be new.

The new engines comply with the Stage V emissions standard, whereas the current engine only complies with the CCNR 1 standard. The reduction in NO_X and PM emissions is therefore 80 % and 97 % respectively as a result of the replacement. The reduction of these two emissions has thus been achieved. The investment in the new engines would amount to approximately EUR 496,350, assuming a price of EUR 450 per kW of installed power. A suitable double-in-single-out gearbox would cost approximately EUR 150,000. The total investment is therefore calculated at EUR 1,646,350.

The previous chapter shows the potential savings on representative trips. In reality, however, ships do not always encounter these particularly favourable conditions and often achieve lower savings over the course of a year. The following figures show the potential fuel savings per year for the Father-Son propulsion system alone, hydrodynamic optimisation alone and a combination of both measures.

12 | Fuel consumption for different configurations. The baseline was *calculated* using the methodology described in 7.2 to take into account the current.

	Yearly fuel consumption [l]	Fuel savings per year [%]	Fuel savings per year [l]
Calculated yearly consumption original vessel	146,873	-	-
Only Father-Son Configuration	137,712	6	8,590
Only Optimized Aft	125,484	15	18,274
Father-Son Configuration and Optimized Aft	116,799	20	23,916

It is therefore evident that the gap to the promised target of a 35 % reduction in CO_2 emissions can vary greatly depending on the perspective: under ideal conditions, only 2 % is missing in the canal to

Funded by the Horizon Europe Programme of the European Union under grant agreement No 101096809
Funded by the Horizon Europe guarantee of the United Kingdom, under project No 10068310
Funded by the Swiss State Secretariat for Education, Research and Innovation

achieve the target with this greening approach (see previous chapter), which does not significantly interfere with ship operations. However, when considering the estimated conditions of more realistic operation, the target becomes more distant, and approximately 15 % of the fuel would need to be replaced by HVO. The implications for costs are demonstrated below:

Blending HVO and diesel on board is currently difficult. As the two fuels are treated differently for tax purposes (diesel for IWT is tax-free and dyed, while HVO is also tax-free for IWT but not dyed), they are not currently permitted to be mixed in the tank and must be purchased as a ready-made blend. The exact blend for this example may not be available everywhere.

The price for marine diesel is assumed to be EUR 0.52, and for HVO EUR 1.20.

13 | Fuel savings and costs for different configurations

	Savings fuel per year [l]	Savings fuel cost per year[€]	HVO needed per year [l]	HVO cost per year [€]	Savings fuel by placing Diesel with HVO [€]
Only Father-Son Configuration	8,590	4,467	39,609	47,531	-43,064
Only Optimized Aft	18,274	9,503	25,645	30,774	-21,271
Father-Son Con-figuration and Optimized Aft	23,916	12,437	16,963	20,356	-7,919

It is immediately clear that, given the assumed ratio of diesel to HVO prices, no satisfactory business case is possible if the shipowner wants to achieve a 35 % reduction in CO_2 emissions. If he/she were to implement the measures and continue to use fossil diesel, the savings would actually contribute to paying off the investment. This can be seen in the column *Savings fuel cost per year[€]*.

If the objectives of the Mannheim Declaration are to be upheld, it will be urgently necessary to significantly increase the energy efficiency of the European inland waterway fleet in the coming years. Since this cannot be achieved through newbuildings alone, the replacement of aft sections must also be considered. On a positive note, financial assistance of up to 80 % of the costs is available in Germany [12]. To make replacement economically attractive even without subsidies, the price ratio of fuel costs must be changed. As soon as HVO is less than 40 % more expensive than diesel (for comparison, in the present example, HVO is 130 % more expensive), savings would be possible while still complying with the targets of the Mannheim Declaration, which would contribute to financing the investment in engines and aft sections.

Funded by the Horizon Europe Programme of the European Union under grant agreement No 101096809
Funded by the Horizon Europe guarantee of the United Kingdom, under project No 10068310
Funded by the Swiss State Secretariat for Education, Research and Innovation

8. Conclusion

This case study showed that with an updated conventional drive system and the optimisation of the hydrodynamics of the aft ship, at the CCNR's targets for 2035 climate-impacting emissions can be achieved with moderate effort. By monitoring the ship, an operational profile was created in which typical operating points could be identified and selected for optimisation. This analysis of the current situation is therefore a very important step in laying the foundation for successful optimisation.

The potential for reducing the power demand by improved hydrodynamics as part of an aft-ship replacement was demonstrated in the current study. Utilising high-fidelity RANS CFD simulations coupled with the parametric model in a fully automated optimisation environment allowed for modelling accurately the complex flow of the hull-propeller-duct interaction under shallow water conditions. By using a tailored actuator disk model suited for ducted propellers and carefully selecting model simplifications an efficient simulation setup was employed which finally led to an efficiency improvement in shallow water of 30 %, while savings of 16 % and 22 % were also achieved in deep and moderate water conditions respectively. Compared to the original geometry of the use case vessel, the shape of the redesigned aft ship shows significant changes in the transom area, the tunnel integration, and the complete frame contour below the tunnel, which mainly controls the propeller inflow.

The success of the multi-object optimizations was underlined by the preceding model test which fully confirmed the improvements achieved. Overall, it was shown that in the context of reducing dependence on fossil fuels, hydrodynamic optimisation can make a significant contribution.

When analysing the operational profile in terms of engine load, canal navigation in particular shows that the large engine operates at a very unfavourable load point there. Significantly more power is required when sailing on the Rhine, making the ship ideal for a concept with two engines of different sizes. The design and analysis of the Father-Son propulsion concept showed that this layout alone can achieve fuel savings of more than 5 %.

The final assessment of the business case showed that, here too, the price difference between fossil and renewable fuels is the decisive factor for refinancing the investment. It would therefore be important to not only introduce subsidy programmes to reduce the investment, but also to align fuel prices, either by imposing sanctions on fossil fuels or by promoting renewable alternatives.

Funded by the Horizon Europe Programme of the European Union under grant agreement No 101096809
Funded by the Horizon Europe guarantee of the United Kingdom, under project No 10068310
Funded by the Swiss State Secretariat for Education, Research and Innovation

9. Literature

[1] 'RESOLUTION No. 92/2 ON NEW CLASSIFICATION OF INLAND WATERWAYS.pdf'. Accessed: Jun. 20, 2025. [Online]. Available: https://www.itf-oecd.org/sites/default/files/docs/wat19922e.pdf

[2] 'Recommended Procedures and Guidelines.pdf'. Accessed: Jun. 20, 2025. [Online]. Available: https://www.ittc.info/media/8007/75-02-02-02.pdf

[3] H. G. Weller, 'Pressure-velocity solution algorithms for transient flows', OpenCFD Ltd., Jul. 2005.

[4] H. G. Weller, 'A New Approach to VOF-based Interface Capturing Methods for Incompressible and Compressible Flow', OpenCFD, 2008.

[5] F. Menter, M. Kuntz, and R. Langtry, 'Ten years of industrial experience with the SST turbulence model', *Heat and Mass Transfer*, vol. 4, Jan. 2003.

[6] B. Friedhoff, K. Hoyer, S. List, and M. Tenzer, 'Investigation of the nominal and effective propeller inflow for a family of inland waterway vessels', *Ocean Engineering*, vol. 187, p. 106180, 2019, doi: https://doi.org/10.1016/j.oceaneng.2019.106180.

[7] W. Lyu, J. Kaufmann, J. Ley, M. Tenzer, and T. Schellin, 'An efficient method to simulate ship self-propulsion in shallow waters and its application to optimize hull lines', *Ocean Engineering*, vol. 312, p. 119328, Sep. 2024, doi: 10.1016/j.oceaneng.2024.119238.

[8] D. B. Spalding, 'A single formula for the "law of the wall"', *Journal of Applied Mechanics*, vol. 28, no. 3, pp. 455–458, Sep. 1961, doi: 10.1115/1.3641728.

[9] K. Michalak and C. Ollivier-Gooch, 'Limiters for unstructured higher-order accurate solutions of the euler equations', *46th AIAA Aerospace Sciences Meeting and Exhibit*, Jan. 2008, doi: 10.2514/6.2008-776.

[10] MAN Truck & Bus SE, 'Marine high speed propulsion engines'. [Online]. Available: https://www.vinkdiesel.nl/images/MAN%20data%20sheets/Marine_Commercial.pdf

[11] Zentralkommission für die Rheinschifffahrt (ZKR), 'Mannheimer Erklärung „150 Jahre Mannheimer Akte - Motor für eine dynamische Rhein- und Binnenschifffahrt"'. Oct. 17, 2018. [Online]. Available: https://www.ccr-zkr.org/files/documents/dmannheim/Mannheimer_Erklaerung_de.pdf

[12] *Richtlinie zur Förderung der nachhaltigen Modernisierung von Binnenschiffen zur Verlagerung von Güterverkehr von der Straße auf die Wasserstraße*. 2023. Accessed: Jun. 23, 2025. [Online]. Available: https://www.elwis.de/DE/Service/Foerderprogramme/Nachhaltige-Modernisierung-von-Binnenschiffen/Richtlinie-Verlagerung.pdf?__blob=publicationFile&v=3

Funded by the Horizon Europe Programme of the European Union under grant agreement No 101096809
Funded by the Horizon Europe guarantee of the United Kingdom, under project No 10068310
Funded by the Swiss State Secretariat for Education, Research and Innovation